REVIEW

Check for updates

Defect-containing metal–organic framework materials for sensor applications

Dahui An,[a] Long Chen, [ID] *[a] Yun Liang,[a] Juan Hou [ID] *[a] and Jiangzhao Chen [ID] *[bc]

Defective metal–organic framework (MOF) materials exhibit remarkable potential across diverse fields such as adsorption, electrocatalysis, and electrochemical sensors due to their exposed massive active sites, defective microstructure, exceptional porosity, substantial specific surface area, and unoccupied metal ligand sites. Herein, the working principles of defect construction, defect mechanism, and defect application of MOFs are first briefly summarized. Therefore, this review enables researchers to be inspired to design defective MOFs for electrochemical sensor applications, which is analyzed to establish a relationship between defect construction, electronic structures, and electrocatalytic performance. To address the current challenging issues of electrochemical sensors, various emerging defect strategies are finally prospected and potential avenues for utilizing defects to enhance sensor technologies are pointed out, providing valuable references for future research.

1. Introduction

In recent years, MOFs have gained widespread attention for their distinctive mechanical, electrochemical, and optical properties, which make them highly promising for various applications, including water electrolysis for hydrogen production, electrochemical sensors, and supercapacitors.[1–4] Since Yaghi *et al.*[5] discovered MOFs in 1999 (Fig. 1b), MOFs have garnered widespread attention among researchers due to their outstanding characteristics, including large specific surface area, tunable pores, designable crystal structures, and abundant active sites.[6] Despite their remarkable properties, MOFs face numerous limitations in electrochemical sensor applications due to their ordered crystalline framework, consisting of metal ions and organic ligands, which can limit MOF adaptability to diverse analytes and sensing conditions, reducing their versatility.[7] Furthermore, pristine MOFs lack intrinsic active sites and constrain the electrochemical sensitivity, particularly in detecting low-concentration analytes or achieving rapid responses.[29] To address these limitations and enhance the sensing capabilities of MOFs, researchers

[a]School of Chemistry and Chemical Engineering/State Key Laboratory Incubation Base for Green Processing of Chemical Engineering, Shihezi University, Shihezi, 832003, China. E-mail: arnoan@qq.com; 2669347572@qq.com; chenlong2012@sinano.ac.cn; hjuan05@shzu.edu.cn

[b]Key Laboratory of Optoelectronic Technology & Systems (Ministry of Education), College of Optoelectronic Engineering, Chongqing University (CQU), Chongqing 400044, China. E-mail: jiangzhaochen@cqu.edu.cn

[c]Faculty of Materials Science and Engineering, Kunming University of Science and Technology, Kunming 650093, China

Dahui An received his bachelor's degree in environmental engineering from Anhui Agriculture University in 2022. He is now a postgraduate student in Chemical Engineering and Technology at Shihezi University under Prof. Chen's supervision. His research interest focuses on MOF materials for electrochemical sensors.

Dahui An

Long Chen received his PhD in material physics and chemistry from the University of Chinese Academy of Sciences (UCAS) in 2016. He is professor at Shihezi University. His current research interests focus on the design and application of inorganic functional materials in the environment and energy conversion and storage including supercapacitors, electrocatalysts, zinc ion-batteries and electrochemical sensors.

Long Chen

have explored various modification methods, including functionalization with different organic groups, metal doping, incorporation of guest molecules, and defect engineering strategies.[8] Functionalization with organic groups, such as carboxylic acids or amine groups, can introduce additional functional sites on surfaces of MOFs, thereby improving their interactions with target analytes. Metal doping involves the substitution of some metal ions within the MOF framework with others, resulting in alterations to the electronic structure and enhanced reactivity. The incorporation of guest molecules into MOF pores creates specific binding sites for analytes, thereby enhancing selectivity. Among these strategies, defect engineering,[20] as depicted in Fig. 1a, has increasingly gained researchers' favor over other modification methods, which not only provides much more active sites compared with alternative approaches,[9] but also stands out in electrochemical performance due to its precision, controllability, and wide applicability.[10] Defect engineering has attracted increasing attention from researchers in various applications such as adsorption, electrocatalysis, and electrochemical detection and has gradually become the preferred choice for MOF modification.

Active defects in MOFs are distinct from the reconstruction process caused by external factors, or internal structural instability in the coordinated environment. These defects are intentionally introduced into MOFs through deliberate and precise design and control. Defective MOFs can be categorized into two main types: metallic defects, which involve the absence of a metal cluster or the substitution of certain metal ions with others in the framework,[25] and conversely, ligand defects,[11,12] which occur when organic ligands are absent or replaced by other small molecules.[26–28] This approach revolves around introducing controlled defects, which play a pivotal role in finely tuning structural,[33] electronic,[34] and various other characteristics of MOFs.[35–37] Defective MOFs present several advantages: (1) expanded surface area and reactivity: defect engineering significantly provides additional adsorption and active sites for target ions to interact with due to the enhanced surface area, which facilitates a more efficient adsorption process;[13–15] (2) abundance of anchoring sites: these additional anchoring sites enable the loading of a greater variety and quantity of MOFs, contributing significantly to enhanced sensing performance;[16,17] (3) expanded sensing range: defects in MOFs significantly alter atomic-level structure–property relationships.[18,19] The presence of defect sites dramatically enhances the permeability of guest molecules,[27,28] including large organic species, through the MOF framework.[21–24] Furthermore, defects enhance charge transport properties of MOFs, further improving their sensing capabilities.[30–32]

Researchers have increasingly employed defect engineering strategies to enhance MOFs' performance across various applications.[134–136] However, compared with gas adsorption and electrocatalytic reactions, the use of defect MOFs in sensor applications has received less attention.[136–139] In this review, we focus on the recent developments in using defective MOFs for optical and electrochemical sensors. The definition, advantages and creation of defectives are summarized. In addition, a comprehensive survey of defective MOF applications for sensors is provided. The design and the primary limitations of defective MOFs for sensor applications, as well as potential avenues for future resolution are analyzed and studied. This review intends to explore potential development prospects of defective MOFs and their derivatives in the field of sensors.

2. Construction and characterization of defective MOFs

Defect engineering can lead to increased adsorption sites,[38,39] improved catalytic performance,[40] and enhanced sensor sensitivity,[41] and there are many ways to introduce defects into the MOF lattice.

Yun Liang received her bachelor's degree in Chemical Engineering and Technology from Yangtze Normal University in 2023. She is now a postgraduate student in Materials and Chemicals at Shihezi University under Prof. Chen's supervision. Her research interest focuses on the design and fabrication of electrolytes and electrode materials and their applications in zinc ion batteries.

Yun Liang

Juan Hou is a professor at the College of Science at Shihezi University. She received her PhD degree from the University of Chinese Academy of Sciences and worked as a postdoctoral researcher at the University of Electronic Science and Technology of China. Her current research interests focus on new photoelectric energy materials and devices.

Juan Hou

Jiangzhao Chen is a professor at the Faculty of Materials Science and Engineering at the Kunming University of Science and Technology. He received his PhD degree from the Huazhong University of Science and Technology and worked as a postdoctoral researcher at Sungkyunkwan University and at the University of Hong Kong, respectively. His current research interests focus on perovskite solar cells.
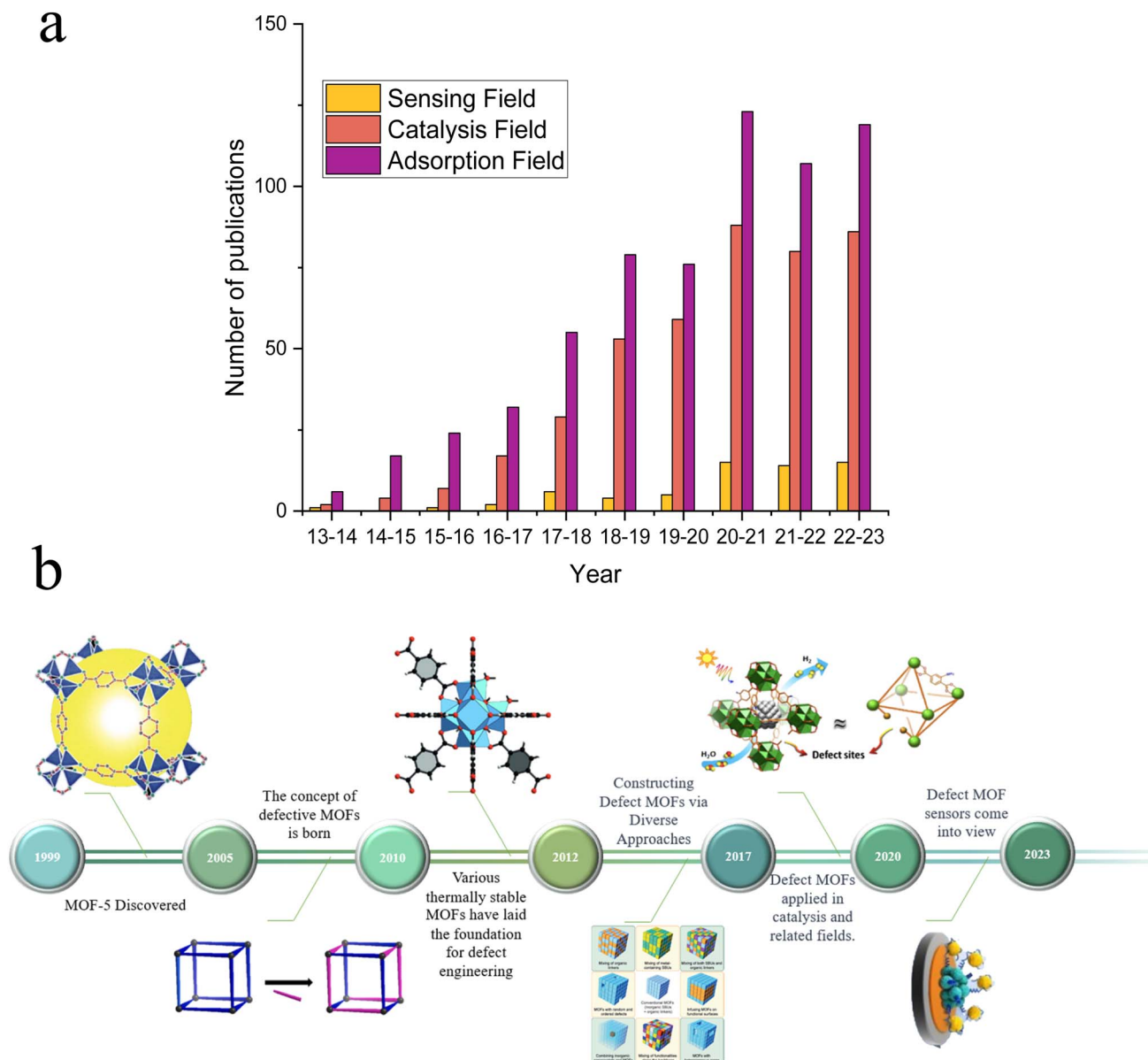
Jiangzhao Chen

Fig. 1 (a) The number of published research articles for the application of defective MOFs in sensing, catalysis, and adsorption fields (data source: Web of Science, retrieved: August 20, 2023). (b) Development of defective MOFs, MOF-5, reproduced with permission.[5] Copyright, 1999, Nature. Defect schematic, reproduced with permission.[106] Copyright, 2023, Elsevier. Defective UIO-66, reproduced with permission.[112] Copyright, 2015, Wiley-VCH. Constructing defect MOFs *via* diverse approaches, reproduced with permission.[113] Copyright, 2017, Elsevier. Catalytic applications of defective MOFs, reproduced with permission.[114] Copyright, 2019, Wiley-VCH. And a defective MOF sensor, reproduced with permission.[93] Copyright, 2023, Elsevier.

With the continuous development of defect engineering for MOFs, the theory of defect construction has become more and more refined. These classifications can be broadly categorized into "*de novo* synthesis (DNS)[25,42] and "post-synthetic treatment (PST).[26,43]" Recent cases of using DNS and PST to construct defective MOFs are shown in Table 1.

2.1 DNS

2.1.1 Defect engineering *via* carboxylic acid modulation. Carboxylic acids including acetic acid (AA),[44] benzoic acid (BA),[45] difluoroacetic acid (DFA),[46] trifluoroacetic acid (TFA),[48] and

others are frequently employed as modulators to introduce defects in MOFs. The acid modulation reaction commences with the rapid formation of metal clusters, initially capped by a soluble, distinct modulator. These clusters are subsequently orchestrated into the final 3D structure through reversible ligand exchange with covalently linked acids.[49,50] In this process, the applied modulators actively participate in the reaction and become integrated into the resultant MOF structure, giving rise to the emergence of structural defects. However, in specific scenarios, these defect-inducing modulators can be eliminated post-synthesis through thermal activation, thereby unveiling the exposed metal sites of the Lewis acid.[51] Shearer

40 | *J. Mater. Chem. A*, 2024, **12**, 38–58

This journal is © The Royal Society of Chemistry 2024

Table 1 Synthesis methods and applications of recently defective MOFs

Defect name	Typical strategies	Defect construction methods	Application areas	References
UIO-66	DNS	Mixed linker	Electrode	120
MOF-74	DNS	Mixed linker	CO_2 capture	123
UIO-67	DNS	Modulation method	Gas adsorption	119
MOF-801	PST	Solvent-assisted linker exchange	Hydrogen restore	121
ZIF-8	DNS	Modulation method	Sensor	122
HKUST-1	PST	Post-synthetic heat treatment	Catalytic conversion	118

et al.[52] explored the impact of carboxylic acid modulators on defect formation within UiO-66. The differences in the structure and composition between the ideal UiO-66 unit cell and those exhibiting missing cluster/linker defects, resulting from the modification, are depicted in Fig. 2a. Their findings revealed that the predominant defect type was cluster defects, and these defects could be controlled by adjusting the acidity and concentration of the modulators.

Feng et al.[53] team corroborated the previous research on defect synthesis using a modulator approach, employing L-proline to synthesize UiO-66 and introduce chiral active sites. Fig. 2b illustrates this process. The modified Zr-MOFs displayed enhanced catalytic activity and diastereoselectivity in aldol reactions, partially attributed to the introduced defects within the MOFs. Peng et al.[47] emphasized the vital role of the modulator approach. They successfully synthesized highly defective UiO-66 by incorporating monocarboxylic acids, partially replacing linkers. Subsequent high-temperature treatment removed modulators, creating multiple open sites within the MOF structure. These defect-induced enhanced adsorption properties effectively removed antimony from real water samples (Fig. 2c).

2.1.2 Defect generation *via* mixed-linker architectures. The mixed linker approach, also a widely adopted strategy in the

Fig. 2 (a) Synthesis of UiO-66 using L-proline as a modulator. Reproduced with permission.[52] Copyright, 2018, Elsevier. (b) Varied adsorption in defect MOFs with different modifiers. Reproduced with permission.[53] Copyright, 2022, Elsevier. (c) Differences in ideal *vs.* defective UiO-66 unit cells. Reproduced with permission.[47] Copyright 2016, American Chemical Society.

DNS methods,[55] involves directly combining two or more organic ligands as precursors during synthesis.[56] This concise and versatile method allows for the intentional introduction of defects, offering new possibilities for tailoring material properties.[57–59]

Using a mixture of ligands, Epp *et al.*[60] synthesized Ru-based MOFs and subsequently explored defect formation in MOFs initiated by crystal growth rates during different synthesis procedures. They systematically investigated the impact of these defects on the structure, morphology, and properties, including catalytic performance, while also studying how various synthesis methods influence the morphologies of MOFs. The change in catalytic properties after the introduction of defects is shown in Fig. 3a. Fan *et al.*[54] applied a mixed-linker defect engineering technique to synthesize Cu(I)-enriched MOFs of the Cu-BTC type. During synthesis, they substituted a portion of the parent linker with truncated pyridine-3,5-dicarboxylate, creating Lewis basic pyridyl sites and reducing carboxyl coordination sites. This modification resulted in the formation of mixed-valence Cu(I)–Cu(II) paddlewheels within the defect-engineered CuBTC structure (Fig. 3b). In another

study, Yu and colleagues[61] used a mixing ligands strategy with Zn^{2+} ions, yielding MOF-derived ZnO nanoclusters with tunable surface oxygen vacancies through annealing. Their findings suggest that coordinate competition can introduce additional unsaturated metal sites in MOFs, resulting in more oxygen vacancies in derived materials. Creating defects in MOFs by mixing the original linker with a second lower-topology linker is a common construction method. Villajos J. A., *et al.*[62] used this approach to synthesize MOFs-74. Higher pK_a and an increased modulator concentration resulted in more defects, providing a simple way to introduce functional sites. As shown in Fig. 3c, a combination of three ligands effectively bound Co ions in the synthesized Co-MOFs-74, generating numerous defects within the material. Therefore, it is an effective means to improve the catalytic and detection performance of MOFs by optimizing ligands.

2.1.3 Defect generation *via* rapid synthesis. The utilization of rapid crystallization techniques, namely microwave-assisted synthesis and high precursor concentration, holds the key to promoting swift MOF crystal formation and effectively introducing defects. These approaches play a crucial role in
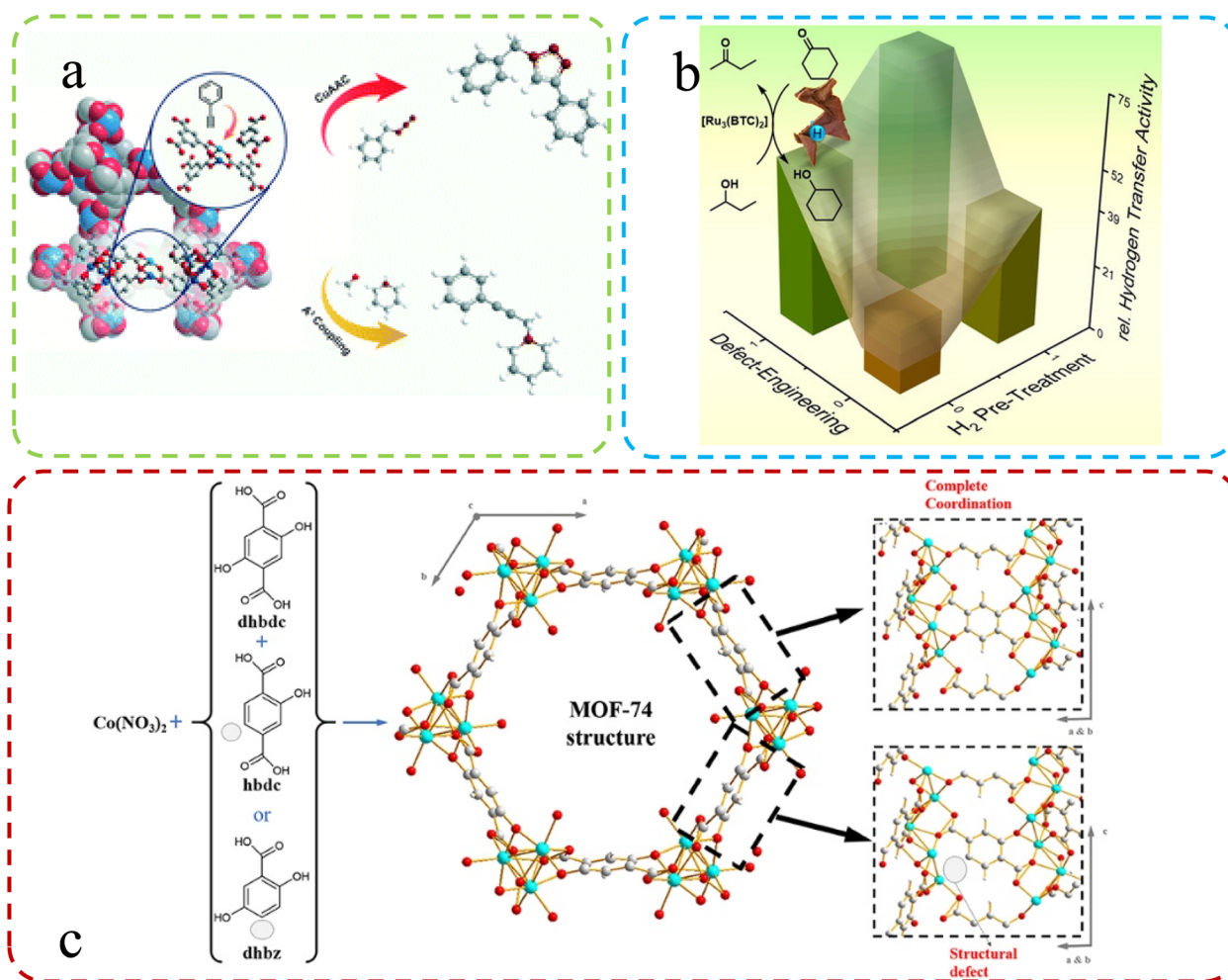

Fig. 3 (a) Schematic illustration of the mixed-linker approach. Reproduced with permission.[60] Copyright, 2021, Royal Society of Chemistry. (b) Defective HKUST-1 synthesized *via* the mixed-linker approach. Reproduced with permission.[54] Copyright, 2020, Wiley-VCH. (c) Generation of structural defects in a MOFs-74 structure by partial linker substitution. Reproduced with permission.[62] Copyright, 2019, Frontiers.

42 | *J. Mater. Chem. A*, 2024, **12**, 38–58

This journal is © The Royal Society of Chemistry 2024

facilitating rapid crystallization while enabling the controlled generation of defects within the MOF crystals.[63] Chaemchuen S. et al.[64] further corroborated this notion, as they emphasized the importance of defect formation induced by the synthesis procedure in MOFs, which delved into the influence of crystallization rate on MOF morphologies and properties, validating the pivotal role of rapid crystallization techniques such as microwave-assisted synthesis and high precursor concentration in enabling controlled defect generation within MOF crystals. As depicted in Fig. 4d, due to the brief synthesis time and rapid reaction rate of microwave-assisted hydrothermal synthesis, certain metal clusters and ligands fail to connect, resulting in the formation of numerous defects highlighted in yellow.

Karimi et al.[65] recently harnessed ultrasonic radiation to synthesize Ce-UiO-66 MOFs with substantial defects, a key factor in enhancing their catalytic performance. Fig. 4b offers a concise overview of these two distinct synthesis methods. The selection of a specific synthesis technique significantly impacts crystal size and defect formation. Crystallization from a quiescent solution tends to produce more extensive crystals, while

agitation can result in smaller crystals with increased defect density. These factors underscore the importance of method choice in tailoring MOF properties for optimal performance.[66]

Rapid synthesis of defective MOFs using solvent-free methods has been favored due to their greenness and rapidity. Ye et al.[67] introduced an environmentally friendly method for rapidly synthesizing solvent-free bimetallic UiO-66(Hf–Zr) MOFs, which exhibited highly dispersed Hf/Zr–OH defect sites. Theoretical calculations showed that rapid synthesis led to an increase in defects (Fig. 4a). The high-concentration, solvent-free synthesis conditions could also be one of the contributing factors to the increased defect formation. Jerozal et al.[104] demonstrated that UIO-66 based on Zr or Hf can autonomously assemble in high-concentration solutions (Fig. 4c). Moreover, in comparison to traditional synthesis methods, the resulting MOFs exhibited a higher prevalence of valeric acid defects. In addition, the fast crystallization time may lead to the assembly of incomplete MOF products, which are inherently more defective than MOF crystals synthesized by slow reactions.[68]
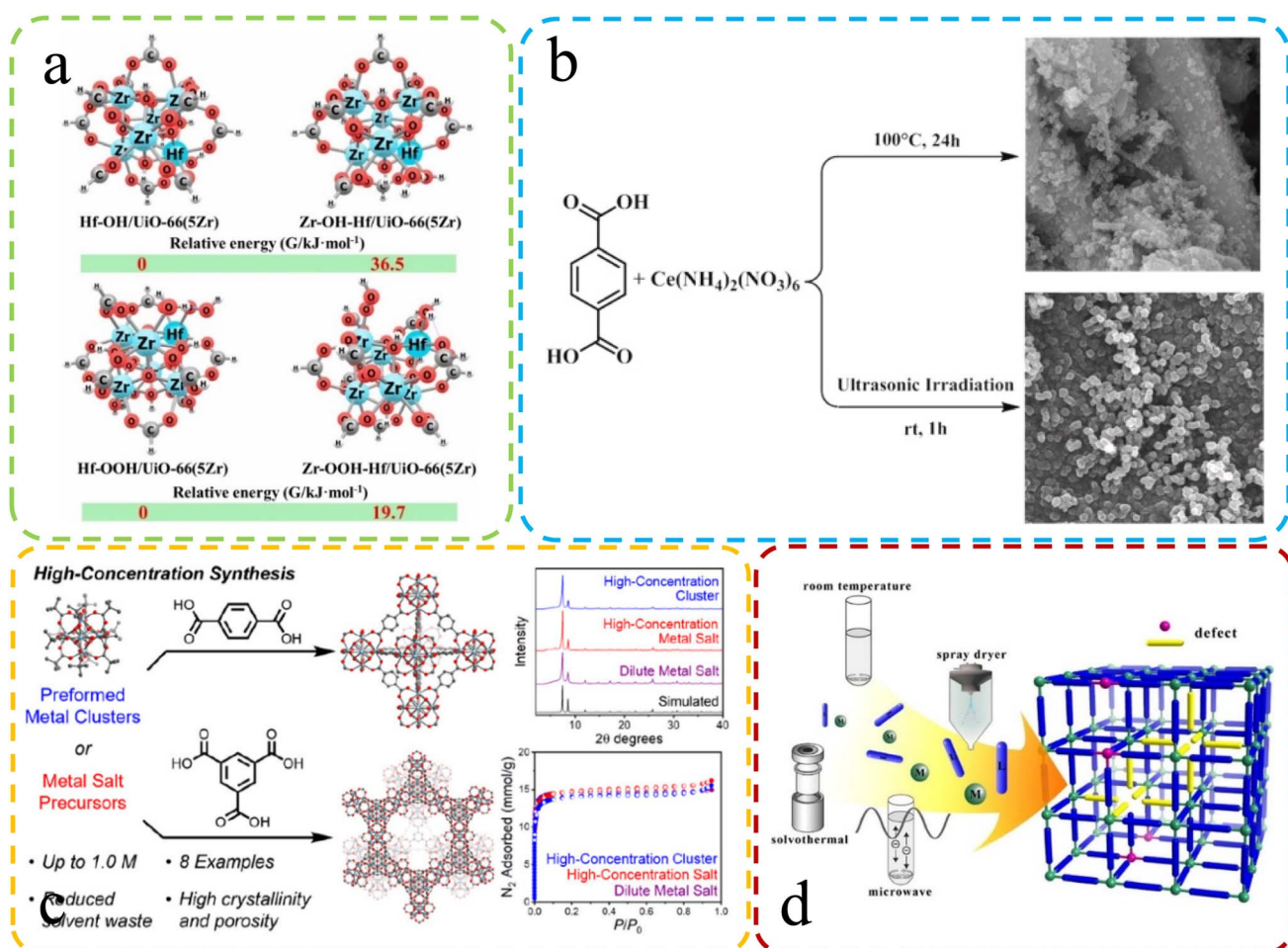

Fig. 4 (a) The difference in Gibbs free energy at different synthesis speeds. Reproduced with permission.[67] Copyright, 2021, Elsevier. (b) Differential SEM characterization of Ce–UiO-66 synthesized via reflux and sonochemical methods. Reproduced with permission.[65] Copyright, 2021, Elsevier. (c) Varied characterization and performance in high-concentration synthesis. Reproduced with permission.[104] Copyright 2022, American Chemical Society. (d) Schematic: fast microwave synthesis of defective MOFs. Reproduced with permission.[64] Copyright, 2017, Elsevier.

This journal is © The Royal Society of Chemistry 2024

J. Mater. Chem. A, 2024, 12, 38–58 | 43

2.2 PST

2.2.1 Defect generation *via* the solvent-assisted linker exchange method. Constructing defects through PST represents a compelling alternative approach. Various methodologies have been successfully employed to introduce mesoporous characteristics into MOFs. Various techniques are employed, including stepwise ligand exchange, chemical etching, thermal decomposition, and phase transformation.[69] Among these, solvent-assisted linker exchange (SALE)[70] is a prominent and well-established post-processing strategy (Fig. 5d), which essentially involves the substitution of MOF linkers with suitably modified or catalytic precursor linkers, subsequently immersed in an appropriate solvent.[71] Kang *et al.*[72] successfully synthesized mesoporous Cu(II)-MOFs, MFM-100, using the SALE method. Scanning electron microscope images (Fig. 5b) clearly illustrate that the morphology of the standard MOFs synthesized significantly differs from that of the MOFs treated with the SALE method. This research employed the SALE method to intentionally introduce crystal defects, emphasizing their role in reshaping the MOFs' structure. As a result, the modified MOFs exhibited exceptional catalytic activity in alcohol oxidation, yielding both high yields and stability. Shearer *et al.*[73] employed the SALE method to synthesize highly porous and defective UiO-66 MOFs. They also introduced the monoethanolamine moiety into the framework through post-

synthetic treatment, replacing bulky benzoate ligands with formate, as depicted in Fig. 5a.

Sanchita Karmakar *et al.*[105] utilized the SALE method to synthesize defective MOF-808-PBA. This intricate integration of methyl viologen generated a sophisticated donor–acceptor composite, akin to an artificial "special pair" at the molecular level (Fig. 5c). This approach allowed for the creation of a unique and advanced molecular structure. Jiang *et al.*[106] introduced a groundbreaking solvent-free and environmentally friendly approach called mechanochemistry-assisted linker exchange (MALE) for post-synthetic modification of MOFs. This innovative method, conducted at room temperature, offers a sustainable alternative to the commonly employed SALE technique. Demonstrated by the efficient exchange of linkers in ZIF-8 using the imidazole-2-formaldehyde (Im-CHO) ligand (Fig. 5e), MALE showcased remarkably faster and more efficient reaction rates compared to traditional SALE. The versatility of the MALE method extended to UiO-66 and diverse functional ZIF-8 analogs, exemplified by ZIF-8/Br, ZIF-8/CF$_3$, ZIF-8/CH$_2$OH, ZIF-8/Cl, and ZIF-8/Et. Notably, ZIF-8/CF$_3$ exhibited enhanced kinetic gas separation performance for C_3H_6/C_3H_8 mixtures.

2.2.2 Defect generation *via* the acid etching method. One method of treating MOFs to introduce defects through acid or base treatment is known as the post-synthetic acid–base treatment approach. In a similar vein, Yang *et al.*[74] employed the
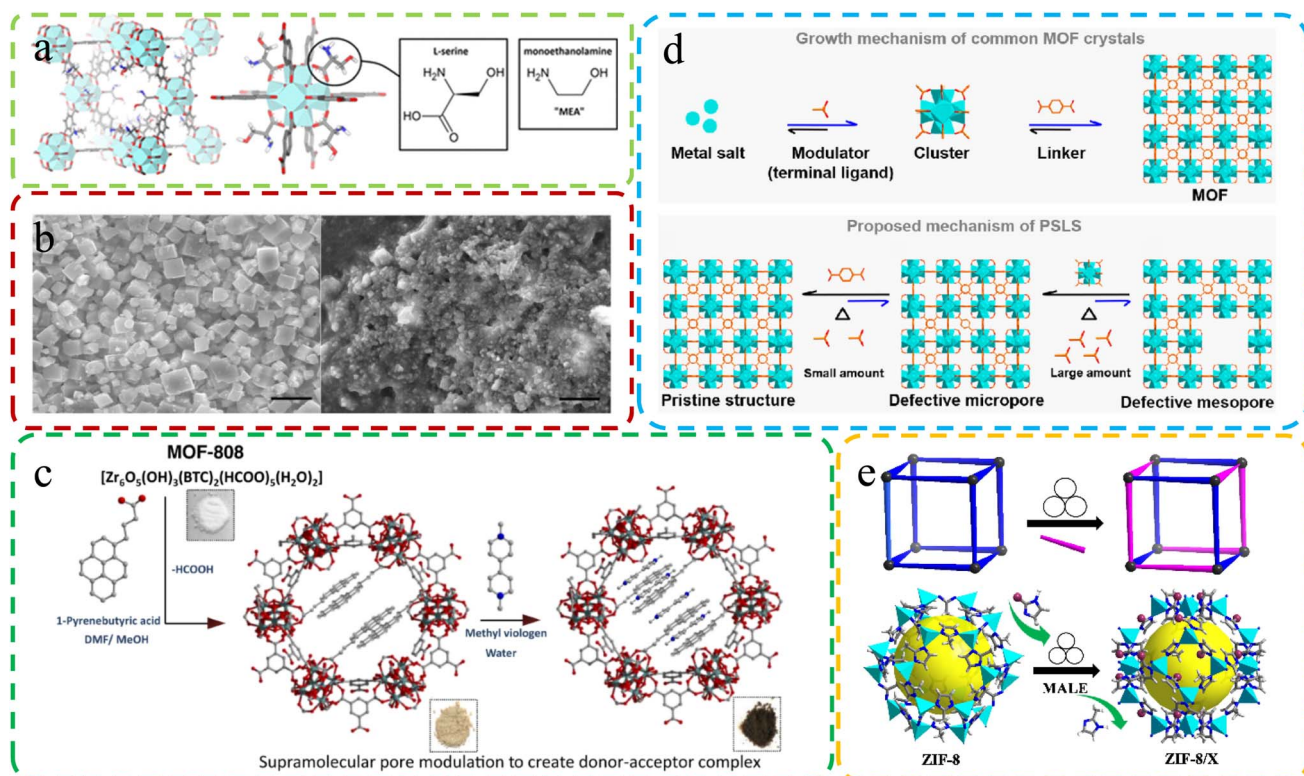

Fig. 5 (a) Molecular structure of defective MOFs with L–serine ligand substitution. Reproduced with permission.[73] Copyright 2016, American Chemical Society. (b) Differences in SEM images of MOFs under different synthesis conditions. Reproduced by permission.[72] Copyright, 2019, Nature. (c) Constructing MOF–808–PBA as the donor, exchanging linkers, and adding MV as the electron acceptor for MOF–808–PBA–MV. Reproduced with permission.[105] Copyright, 2023, Nature. (d) Crystal generation: common MOFs (above) *vs.* SALE method (below). Reproduced with permission.[115] Copyright 2022, American Chemical Society. (e) Schematic diagram of the MALE method. Reproduced with permission.[106] Copyright, 2023, Elsevier.

44 | *J. Mater. Chem. A*, 2024, **12**, 38–58

This journal is © The Royal Society of Chemistry 2024

monocarboxylic acid etching strategy to introduce defect engineering in Zr-based UiO-66 MOFs, transforming them into hierarchical porous counterparts. This defect engineering process, illustrated in Fig. 6a, evolves with different etching times, removing partial ligands and metal clusters to create mesopores within the MOFs. The precise control of MA concentration and reaction temperature allows tailored manipulation of textural attributes such as pore size distribution, surface area, and pore volume. These hierarchically porous MOFs, a product of defect engineering, inherit the exceptional stability of UiO-66 and exhibit remarkable adsorption behavior toward enzymes of varying sizes.
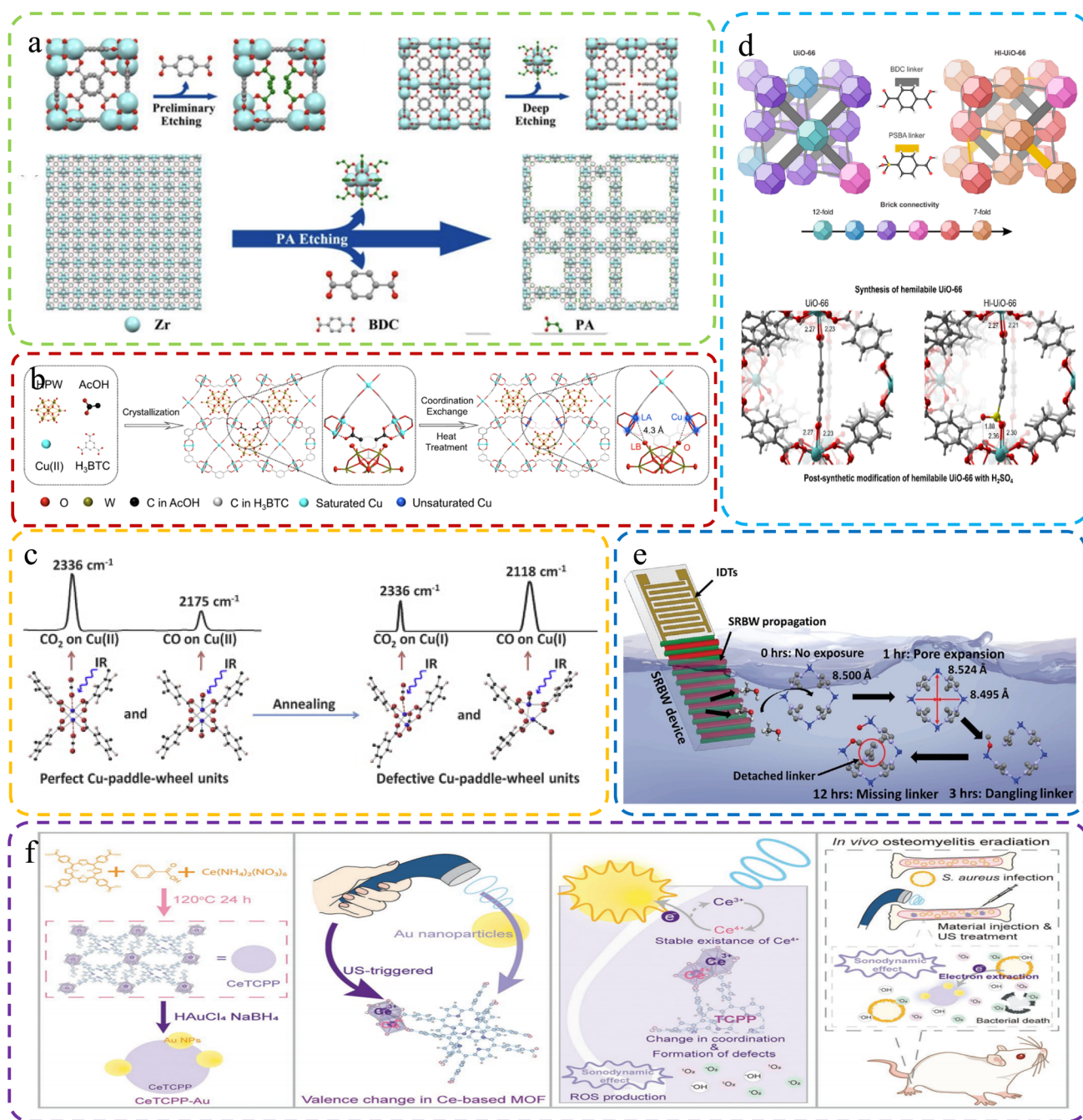

Fig. 6 (a) Creating hierarchical porous Zr-based MOFs *via* monocarboxylic acid etching with propionic acid etching. Reproduced with permission.[74] Copyright, 2018, Wiley-VCH. (b) Creating Dx-NENU-3 with FLP sites *via* coordination defect engineering. Reproduced with permission.[107] Copyright, 2023, Wiley-VCH. (c) Structural and characterization changes of MOFs and defective MOFs after heat treatment. Reproduced with permission.[76] Copyright, 2015, Elsevier. (d) Top: UiO-66 and Hl-UiO-66 with varied brick configurations, creating unsaturated Zr sites. Bottom: UiO-66 with one missing linker and Hl-UiO-66 with one missing linker and one PSBA linker. Reproduced with permission.[108] Copyright 2020, American Chemical Society. (e) Schematic of the setup for acoustomicrofluidic defect creation. Reproduced with permission.[109] Copyright, 2023, Wiley-VCH. (f) CeTCPP-Au for US-triggered Au NP electron trapping, enhancing SDT for bacterial eradication and osteomyelitis detection. Reproduced with permission.[116] Copyright, 2023, Wiley-VCH.

2.2.3 Defect induction *via* thermal treatment. Thermal treatment is another commonly used method for constructing defects. Szanyi and collaborators[75] ascertained that through postsynthetic thermal treatments, Cu(ɪɪ) dimers within the HKUST-1 framework can undergo reduction to Cu(ɪ). This transformation engenders the formation of defects, resulting in the coexistence of Cu(ɪ) and Cu(ɪɪ) entities within the hybrid architecture. Moreover, these processes augment the population of active sites within the material, leading to enhanced catalytic performance. Furthermore, alongside alterations in the metal clusters, thermal treatment frequently induces modifications in the ligand constituents within the MOF structure, consequently giving rise to the emergence of structural defects. Liang *et al.*[107] introduced defects into a polyoxometalate-based MOF through controlled thermal treatment (Fig. 6b). This defect engineering resulted in the creation of Lewis acid sites at metal nodes and Lewis base sites on the polyoxometalate's surface. These structural modifications, made possible by the compatibility between the polyoxometalate and MOF, had a significant impact. The resulting MOF, strategically endowed with defects, exhibited a substantial improvement in catalytic activity in acetylene semihydrogenation. This enhancement can be attributed to the synergistic effects of these defects. Wang *et al.*[76] innovatively introduced tunable coordinative defects in UHM-3 surface-mounted MOFs. Using a room-temperature liquid phase epitaxy method, they created highly homogeneous UHM-3 MOF thin films on a solid substrate with minimal defects. Subsequently, controlled thermal post-synthetic treatment induced Cu(ɪ) defect sites, strategically enhancing MOF properties (Fig. 6c). In a similar study, Feng *et al.*[108] employed thermal and post-synthetic treatments to enhance the catalytic performance of UiO-66 by introducing defects into the framework. Through controlled heat treatment and treatment in H_2SO_4, they created a highly defective UiO-66 material, denoted as Hl-UiO-66-SO$_4$ (Fig. 6d). This synthesis maintained a three-dimensional UiO-66 network, with the highest defect concentration also correlating with the highest stability. The highest defect concentration not only exhibited superior stability but also demonstrated outstanding catalytic performance.

2.2.4 Defect introduction *via* the ultrasonic-assisted method. In a study by Massahud and colleagues,[109] they explored the manipulation of MOF properties through defect engineering. However, achieving defects in ZIF-8 is challenging due to its stability. The researchers found that applying high-frequency hybrid acoustic waves in a liquid pressure medium can induce permanent structural changes in ZIF-8 crystals. This process enhances the diffusive transport of guest molecules, expanding the pore framework and creating defects (Fig. 6e). It demonstrates the potential for tailored defect engineering in MOFs through acoustic exposure time and practical application, including solvent-assisted ligand exchange for various crystal sizes, while preserving framework porosity and structural integrity. Building upon the concept of manipulating MOFs through defect engineering, a subsequent breakthrough study by Zheng and team[116] delved into the realm of precisely tuning catalytic properties using innovative techniques. They explored the fascinating realm of defect engineering within MOFs to precisely tune their catalytic properties. To achieve precise defect control, they employed a cerium-based MOF (CeTCPP) decorated with gold nanoparticles. Ultrasound irradiation of these gold nanoparticles selectively converted one-third of the original Ce^{3+} nodes into Ce^{4+}, inducing structural irregularities in the CeTCPP-Au framework. This reconfiguration hindered electron–hole recombination, ultimately enhancing the production of reactive oxygen species. These favorable defects improved the selectivity against *Staphylococcus aureus* and *Escherichia coli*, showing promise for osteomyelitis therapy (Fig. 6f).

DNS is the method that involves the incorporation of active sites directly into the MOFs' structure during the synthesis process. This is achieved by introducing unstable small molecule ligands that can be easily removed before catalysis, leaving behind coordinated unsaturated metal ion centers. DNS is known for its convenience, as it streamlines the process of introducing defects during MOF formation. It is particularly useful when specific defect types or configurations are desired. However, one limitation of DNS is that it may lack precise control over the final configuration of the defects, and the outcome can sometimes be unpredictable.[77]

In contrast, PST is an approach that aims to introduce defects or functional groups after the MOFs' formation. This is achieved by employing various techniques under extreme conditions, such as harsh washing, ball milling, acid treatments, or plasma treatment. PST provides a high degree of control over the type and location of defects introduced into the MOFs. It allows for tailored defect engineering while preserving the original MOF structure and stability. PST is particularly effective when precise control over defect characteristics is essential for specific applications.

Both DNS and PST have their merits and considerations. The choice between them depends on the specific application and the desired level of control over defect characteristics in the MOFs. DNS offers convenience during MOF synthesis, while PST provides precision in defect engineering. Understanding the mechanisms underlying these synthesis methods is crucial for advancing research on MOF synthesis.

2.3 Characterisation of defective MOFs

To attain a comprehensive understanding of the defect coordination environment within MOFs, it is imperative to provide a detailed overview of characterization techniques. These techniques play a crucial role in revealing valuable insights into various aspects of defect sites, including their type, location, and quantity.[124] Various techniques have been employed to detect defects in MOFs, primarily including X-ray diffraction (XRD), high-resolution transmission electron microscopy (HRTEM), thermal gravimetric analysis (TG), nuclear magnetic resonance (NMR), Fourier transform infrared spectroscopy (FTIR), electron paramagnetic resonance (EPR), and more.

XRD is a key technology for identifying lattice defects in MOFs, used to detect anomalies such as vacancies, dislocations, or other lattice irregularities. This method hinges on analyzing
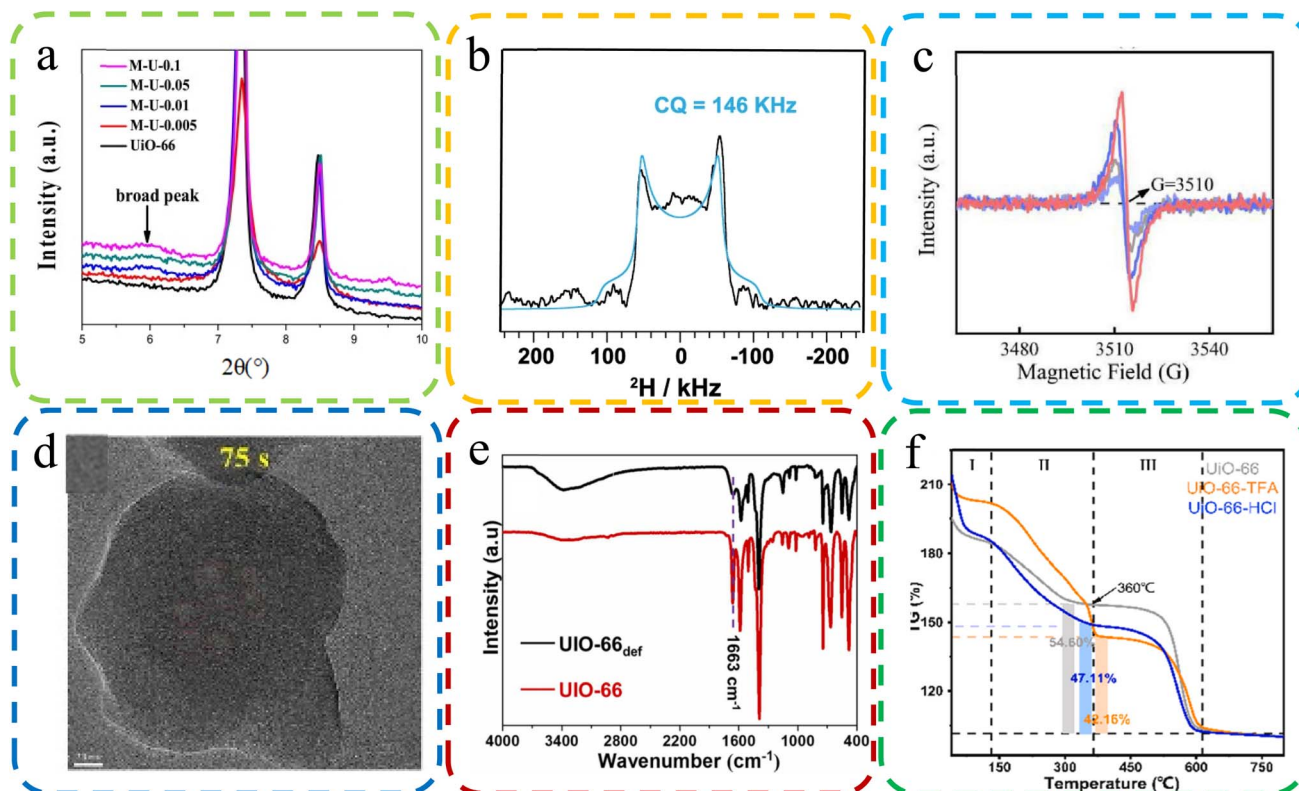
46 | *J. Mater. Chem. A*, 2024, **12**, 38–58

This journal is © The Royal Society of Chemistry 2024

Fig. 7 (a) XRD images with some missing linker defective UiO-66. Reproduced with permission.[125] Copyright, 2019, Elsevier. (b) An NMR map of MOF-74 in the presence of a formate deficiency. Reproduced with permission.[127] Copyright, 2023, Nature Communications. (c) EPR spectra of the oxygen-vacancy content of UiO-66-TFA. Reproduced with permission.[47] Copyright, 2022, Elsevier. (d) HRTEM was applied to visualize the ZIF-7 sample defects. Reproduced with permission.[126] Copyright, 2023, Elsevier. (e) FT-IR spectra of UIO-66 and cluster defects UIO-66 def. Reproduced with permission.[128] Copyright, 2023, Elsevier. (f) TGA plots of body weight loss by UiO-66, UiO-66-TFA, and UiO-6-6-HCl. Reproduced with permission.[129] Copyright, 2023, Elsevier.

the diffraction patterns arising from X-ray interactions with the crystalline matrix of MOFs. Perturbations in these patterns due to lattice defects are discernible through meticulous analysis. Zhang *et al.*, employed XRD to detect missing linker defects in modified UiO-66, which was evidenced by the deviation in diffraction patterns, most notably a broad peak at $2\theta = 5$–7 °C, divergent from that of standard UiO-66, as elucidated in Fig. 7A.[125]

NMR spectroscopy serves as a robust tool for detecting and quantifying molecular-level defects in MOFs, particularly in discerning variations in functional groups and linkers. Anomalies in the NMR spectrum, such as shifts in peak positions, indicate the presence of defects. In recent research, Fu *et al.* leveraged solid-state 2H NMR on MOF-74, uncovering formate defects originating from DMF. This was inferred from a distinct broad 2H quadrupolar pattern, as delineated in Fig. 7B.[127]

EPR spectroscopy is instrumental in the identification of paramagnetic defects, such as unpaired electrons or oxygen vacancies within MOFs. EPR mainly determines the formation of defects *via* the interaction strength between magnetic moment and electromagnetic radiation. Peng *et al.* utilized EPR to probe oxygen vacancies in MOFs, observing symmetrical signals around 3510 G in UiO-66-TFA, the hallmark of oxygen vacancies, as depicted in Fig. 7C.[47]

HRTEM offers a profound visualization of the microstructure of MOFs, including explicit characterization of lattice defects. It provides high-resolution imagery that elucidates the location, morphology, and density of defects. Chen *et al.* utilized HRTEM to examine ZIF-7 samples, unearthing voids indicative of structural defects, as shown in Fig. 7D.[126]

FT-IR spectroscopy is a pivotal method for detecting structural defects in MOFs by scrutinizing vibrational modes. Alterations in the FT-IR spectrum, such as the broadening or shifting of peaks, are suggestive of defects. Kar *et al.* compared the FT-IR spectra of UIO-66 and UIO-66def, which revealed marked discrepancies, particularly in the –CO stretching peak at 1663 cm^{-1}, indicative of structural defects, as evidenced in Fig. 7E.[128]

TGA is an essential technique for identifying defects in MOFs, achieved by analyzing weight loss patterns correlated with defect density. It methodically tracks weight loss during thermal treatment, with deviations from expected patterns signaling the presence of defects. Peng *et al.* employed TGA to evaluate the thermal stability of MOFs, which indicated the higher incidence of ligand defects in UiO-66-TFA compared to UiO-66-HCl, as illustrated in Fig. 7F.[129]

Beyond the primary characterization techniques outlined earlier, an array of supplementary methods stands to augment

This journal is © The Royal Society of Chemistry 2024

J. Mater. Chem. A, 2024, **12**, 38–58 | **47**

our comprehensive understanding of defects in MOFs. These additional techniques include high-resolution neutron powder diffraction (HRNPD),[130] electrospray ionization mass spectrometry (ESI-MS),[131] atomic force microscopy (AFM),[132] and confocal fluorescence microscopy (CFM),[133] alongside the strategic integration of multiple approaches. Each of these methods provides distinct and invaluable insights into the nature, distribution, and typology of defects within MOFs, thereby enriching our understanding of their structural complexities.

At its core, the characterization of structural defects in MOFs is a multifaceted task that demands the deployment of a diverse spectrum of analytical tools, each grounded in unique operational principles. By harnessing the strengths of these primary and supplementary techniques, researchers are equipped to construct a holistic view of defective MOF architectures. This enriched perspective is pivotal in demystifying the intricate ways in which defects influence the properties and applications of MOFs, thereby catalyzing progress in the realm of MOF research.

3. Defective MOFs: advancing sensor innovations

Introducing defects into MOFs has become an effective strategy for improving their detection performance. This seemingly counterintuitive approach is underpinned by a range of intricate mechanisms that collectively contribute to the improved sensing capabilities of these materials.[78] Defect sites can introduce additional active sites that increase the material's capacity for adsorption and reactivity with the target molecule, thereby enhancing its performance. However, it is important to acknowledge that these defect sites may also lead to structural instability in the material, which can reduce its overall durability and long-term viability.[79] Researchers must carefully balance the trade-off between the performance improvements gained through defect engineering and the potential consequences of structural instability.

Defects in MOFs can create localized disruptions in the regular crystalline structure, leading to a myriad of effects that synergistically amplify detection performance.[80] One key mechanism is the increased availability of active sites. Defects often create vacant sites or unsaturated metal centers, serving as preferred binding sites for target analytes. This enhanced availability of binding sites facilitates a higher degree of interaction between MOFs and analyte molecules, leading to heightened sensitivity in detection. Furthermore, defects can significantly alter the surface properties of MOFs. These structural irregularities translate into a larger surface area, effectively providing more room for molecules to adsorb and participate in chemical reactions. As a result, MOFs with defects can accommodate a larger quantity of analytes, leading to amplified signals and improved detectability.[81]

The introduction of defects can also influence the diffusion kinetics of molecules within the MOF framework. Defects can create more accessible diffusion pathways, enabling faster and more efficient movement of analytes to active sites.[82] This streamlined diffusion enhances the response time of the sensing process, allowing for rapid and accurate detection. Another critical aspect is the modulation of electronic properties.[83] Defects can introduce energy levels within the MOFs' electronic band structure, leading to altered charge transfer and electronic interactions.[84] These changes can enhance the affinity of the MOFs for specific analytes, resulting in increased selectivity and sensitivity.[85]

However, it's essential to note that defects can induce structural strain, which imparts mechanical flexibility to MOFs. While this flexibility can enable conformational changes upon analyte binding, leading to a measurable signal change that is essential for certain sensing mechanisms, it can also contribute to the overall structural instability of the material. This potential instability may limit the material's long-term viability and durability.[86]

Importantly, defects can be tailored and engineered to elicit specific responses to target analytes.[87–89] Through deliberate defect design, researchers can customize MOFs for diverse applications, spanning environmental monitoring to medical diagnostics. In conclusion, the introduction of defects in MOFs represents a sophisticated approach to boost detection performance, but it should be approached with careful consideration of the potential trade-offs. Through mechanisms such as increased active sites, enhanced surface area, altered diffusion kinetics, and modified electronic properties, defects synergistically enhance the interactions between MOFs and analytes. This results in improved sensitivity, selectivity, and response time, making defect-engineered MOFs highly promising for advanced sensing technologies.

3.1 Advanced biosensing

Biological molecules are fundamental building blocks that underpin the complexity and functioning of living organisms. Understanding and analyzing these molecules are crucial for various scientific disciplines, from medicine and biotechnology to environmental monitoring and food safety. As the intricacies of biological processes continue to be unraveled, the need for sensitive and specific detection methods becomes increasingly apparent. Biosensing, which accurately detects and quantifies biological molecules, is now vital in modern research and applications. Defective MOFs have garnered significant attention due to their substantial specific surface area, rendering them promising candidates as carriers for nanocrystal immobilization, thus emerging as prospective materials for the detection of small biological molecules.

Tian et al.[93] utilized a diverse ligand synthesis approach to create an efficient electrochemical autosensing method for Staphylococcus aureus detection. They employed mixed ligands to synthesize copper-based metal–organic frameworks encapsulated with Cu_2O nanocrystals (ML-Cu_2O@Cu-MOFs). These nanospheres, featuring multiple Cu valence states and a defect-rich crystal structure, exhibited high catalytic activity for thiamine hydrochloride and hydrogen peroxide (H_2O_2) assays. The sensor demonstrated low detection limits for thiamine hydrochloride and H_2O_2, along with robust stability and

48 | J. Mater. Chem. A, 2024, 12, 38–58

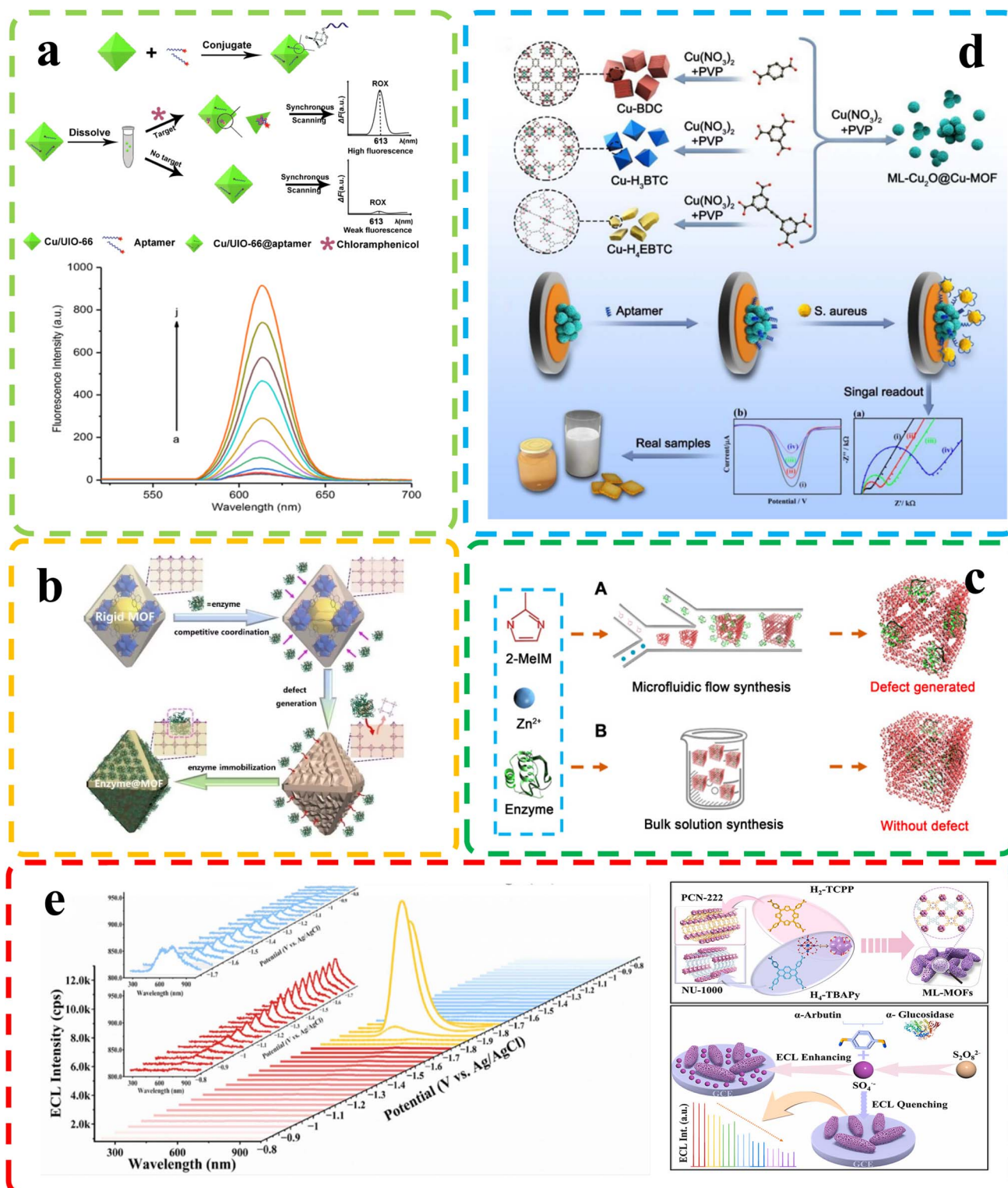This journal is © The Royal Society of Chemistry 2024

Fig. 8 (a) Top: chloramphenicol detection principle; bottom: fluorescence of chloramphenicol at different concentrations. Reproduced with permission.[102] Copyright, 2020, Nature. (b) Dynamic defect generation for enzyme immobilization *via* MOF dissociation equilibrium. Reproduced with permission.[110] Copyright, 2023, Wiley-VCH. (c) Enzyme-MOF composite synthesis. Reproduced with permission.[117] Copyright, 2020, Science. (d) Top: Cu-MOF-based *Staphylococcus aureus* biosensor; bottom: electrochemical biosensor with ML-Cu$_2$O@Cu-MOFs for *Staphylococcus aureus*. Reproduced with permission.[93] Copyright, 2023, Elsevier. (e) Top: ECL spectra of M6-MOFs on a GCE with K$_2$S$_2$O$_8$; insets show spooled ECL spectra: red for evolution and blue for devolution. Bottom: M6-MOF preparation. Reproduced with permission.[111] Copyright, 2023, Elsevier.

reproducibility (Fig. 8d). This biosensor based on ML-Cu$_2$O@Cu-MOFs offers a promising approach for foodborne bacteria analysis and food safety assessment. Lu et al.[102] developed a fluorescence-based method for quantitative chloramphenicol (CAP) detection using Cu/UiO-66, a bimetallic organic framework nanomaterial. Fig. 8a illustrates the concept of performance improvement before and after defect introduction. They employed double-labeled aptamers of CAP with phosphate and the fluorescent dye 6-carboxy-x-rhodamine (ROX). In the absence of CAP, Cu/UiO-66 quenched ROX fluorescence *via* photoinduced electron transfer. However, the presence of CAP induced a change in the aptamers' spatial structure, leading to ROX fluorescence recovery. This method demonstrated high sensitivity, selectivity, and a low detection limit of 0.09 nmol L^{-1}, enabling precise CAP quantification. Enzyme immobilization enhances enzyme stability and activity by affixing them to a carrier. This technique improves biosensor sensitivity in complex environments, expanding its effectiveness in detecting a wider range of analytes (Fig. 8c depicts common methods of immobilizing enzymes using defective MOFs). However, conventional carrier materials might encounter limitations in certain scenarios, where in this interdisciplinary field, defect-engineered MOFs are emerging as a novel class of materials. In a related study, Feng et al.[110] present an innovative dynamic strategy for enzyme immobilization within MOFs to address challenges in industrializing bioactive molecules. This approach leverages enzyme-mediated MOF dissociation, with enzymes acting as "macro ligands," competing with original ligands. This competition triggers metal cluster release within MOFs, generating defects and facilitating gradual enzyme transport from surface to interior. Consequently, various enzymes can efficiently immobilize within MOFs, creating composites with robust enzymatic activities, protection, and high reusability (Fig. 8b). This method revolutionizes enzyme immobilization and enables efficient multienzyme bioreactors for cascade reactions. Meanwhile, in another sensor study that investigated enzyme concentration, Shao and colleagues[111] demonstrated a novel approach to tackle the challenges of conductivity and emission efficiency in MOFs, which often limit their effectiveness in electrogenerated chemiluminescence (ECL) sensing applications. They achieved this by ingeniously combining an electroactive linker (H$_2$-TCPP) with an ECL-active electrogenerated chemiluminescence linker (H$_4$-TBAPy), resulting in the creation of mixed-linker defective ML-MOFs with significantly enhanced photoelectrochemical activity (Fig. 8e). Notably, the leading ML-MOF variant, denoted as M6-MOFs, exhibits a remarkable 15.4-fold improvement in ECL performance compared to single-linker MOFs. Equally impressive is the M6-MOFs' ECL efficiency, which boasts a remarkable 73-fold enhancement over commercial Ru(bpy)$_3^{2+}$. This exceptional enhancement is attributed to the synergistic interplay between the two distinct linkers. Remarkably, researchers leverage M6-MOFs as a potent ECLphore, showcasing their capacity for sensitive and selective α-glucosidase detection. The applicability of this system extends to human serum samples, offering promising practicality. This work not only pioneers the advancement of MOFs' conductivity and ECL efficiency through

strategic linker amalgamation and bandgap manipulation but also underscores the immense potential of defect-engineered MOFs for advanced ECL sensing applications.

3.2 Enhanced chemical sensing

Chemical molecules, both natural and synthetic, surround us in our daily lives and profoundly impact human health and the environment. The potential hazards posed by these molecules demand vigilant monitoring and accurate detection methods. Analyzing and identifying harmful chemical species is critical for ensuring public safety, environmental preservation, and the quality of various products. As scientific knowledge continues to evolve, the need for enhanced chemical sensing technologies becomes increasingly apparent. These innovative sensing methods hold the key to more effectively and efficiently detecting hazardous chemicals, leading to improved risk assessment, timely interventions, and better mitigation strategies.

Sha and his team[92] (Fig. 9b) focused on constructing defect-engineered MOFs with histidine-functionalized active sites (His-MIL-101) by the missing linker strategy. His-MIL-101 with a histidine unit in the iron active site exhibited double the peroxidase-like activity of parent MOFs. The introduction of histidine increased the specific surface area and provided an optimized electronic structure for active sites, promoting the generation of active intermediates (hydroxyl radicals). A His-MIL-101-based colorimetric biosensing platform was designed to accurately detect metallothioneins, demonstrating a wide detection range from 20 nM to 50 μM and a low detection limit of 10.49 nM.

Researchers led by Wu developed high-performance humidity sensors using ionic liquid-modified MOF-derived polymer films.[95]

The preparation of the material and the mechanism of humidity detection are shown in Fig. 9c. By introducing defect engineering, they uniformly incorporated the ionic liquid ligand into the frameworks of UIO-66, resulting in a significant enhancement of hydrophilicity in the sensing materials. These defects enhanced adsorption and desorption properties, enabling the synthesis of functional MOF-based films *via in situ* photoinduced thiol–ene click reactions. The humidity sensor excelled in the 5% RH – 30% RH range, showing minimal hysteresis (approximately 0.2% RH) and rapid response/recovery times (0.6 s/1.7 s). Missing-linker defects facilitate analyte desorption kinetics, resulting in faster sensor recovery. Zhang et al.[99] developed a method to fabricate microporous MOFs as efficient chemical sensors. They assembled UiO-66 crystals with controlled sizes and introduced missing-linker defects to create MOF optical sensors with adjustable optical properties. The sensors displayed rapid response (2.00 s) and short recovery times (3.00 s) to ethanol vapor. Mesoporous features significantly improved sensitivity (~24.6% for saturated ethanol vapor), response speed (~42.9%), and recovery speed (~59.7%) compared to dense counterparts. Crystal size mildly influenced response speed but had a more profound effect. Crystal sizes mildly influence response speed but
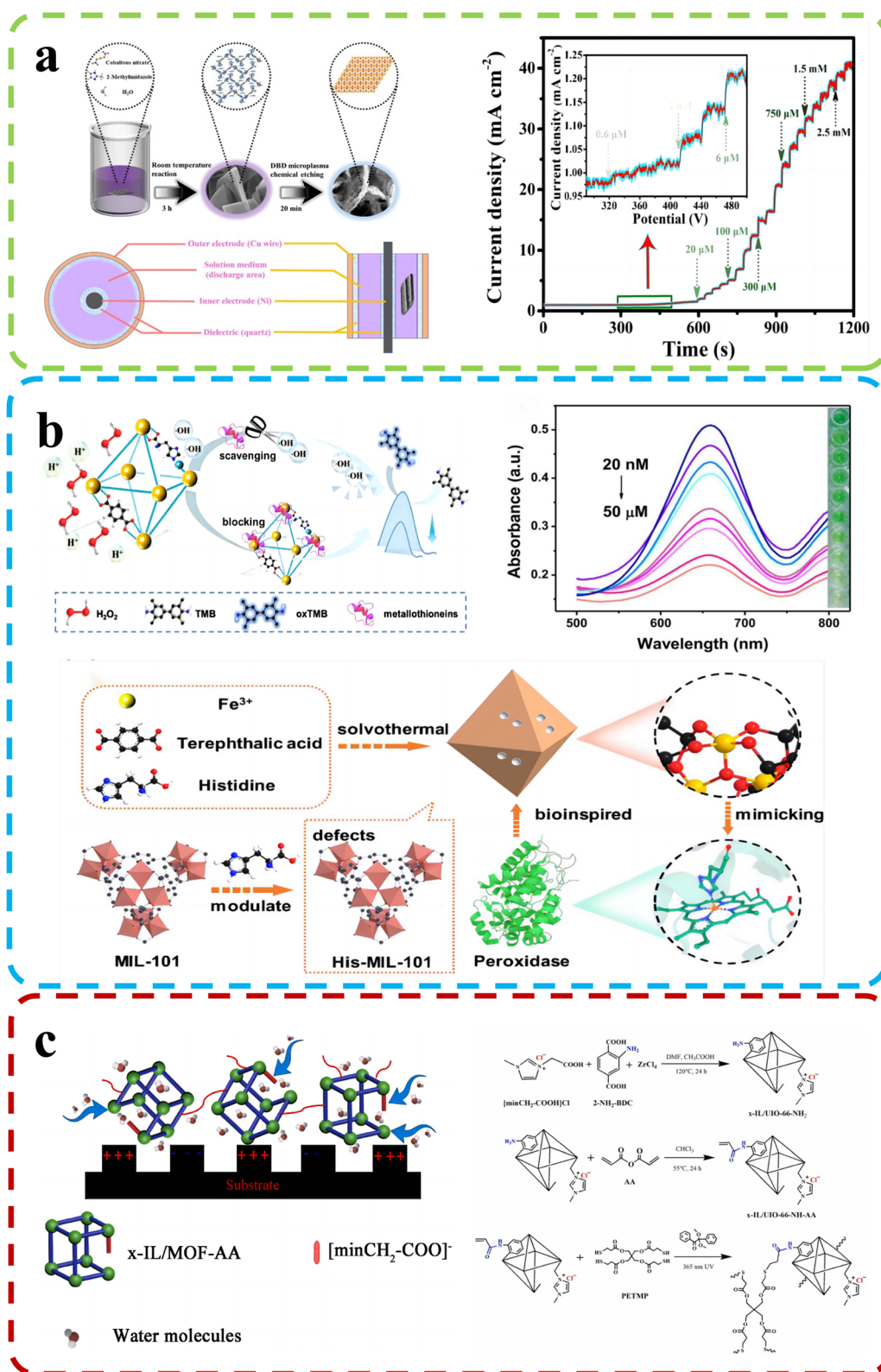
50 | *J. Mater. Chem. A*, 2024, **12**, 38–58

This journal is © The Royal Society of Chemistry 2024

Fig. 9 (a) Top: D-Co(OH)$_2$ synthesis schematic and DBD reactor device structure. Bottom: Amperometric (i−t) curve of D-Co(OH)$_2$/CC (applied potential: −0.2 V). Reproduced with permission.[92] Copyright, 2022, Elsevier. (b) Top: the His-MIL-101 mechanism and performance for metallothionein detection. Bottom: Synthesis of His-MIL-101. Reproduced with permission.[91] Copyright, 2022, Elsevier. (c) Top: Humidity sensing mechanism. Bottom: MOF-based polyelectrolyte synthesis. Reproduced with permission.[95] Copyright, 2022, Elsevier.

profoundly affect it. Similarly, under the guidance of defect engineering, Kang and their colleagues[97] successfully synthesized highly stable 3D MOFs, namely DUT-67(Hf) and DUT-67(Zr), through a solvothermal reaction. These defect-rich MOFs demonstrated excellent proton conductivities and were employed as highly sensitive room temperature sensors for detecting ammonia. Under various relative humidity conditions (68%, 85%, and 98% RH), the sensors exhibited remarkable stability and sensitivity in the detection of volatile amine gases, with impressive detection limits of 0.5 ppm for methylamine, dimethylamine, and trimethylamine. Furthermore, derivatives of defect-rich MOFs have also exhibited exceptional sensing performance. For instance, Hu et al.[91] created a defect-rich $Co(OH)_2$ nanoenzyme sensor from MOF-derived cobalt via a room-temperature reaction and chemical etching with dielectric barrier discharge microplasma (Fig. 9a). It displayed superior catalytic activity for thiamine hydrochloride and hydrogen peroxide (H_2O_2) assays, with detection ranges of 0.0006 mM to 2.75 mM for thiamine hydrochloride and 0.001 mM to 5.5 mM for H_2O_2. The sensor also achieved low limits of detection at 14 nM for thiamine hydrochloride and 93 nM for H_2O_2. Its long-term durability exceeded 25 days, maintaining high sensitivity for TCL and H_2O_2 assays.

3.3 Environmental sensing

The environment, with its intricate web of ecosystems and natural processes, serves as the life-supporting foundation of our planet's biosphere. It sustains an incredible diversity of living organisms and provides vital resources essential for human well-being. However, in recent times, escalating anthropogenic activities have posed unprecedented challenges to environmental integrity, necessitating a deeper understanding and effective monitoring of environmental changes. By harnessing innovative sensing technologies, we can gain invaluable insights into environmental parameters, assess ecosystem health, and devise informed strategies for conservation and sustainable resource management. Defect-rich MOFs may help mitigate pesticide residue's environmental impact on human health.

Yan et al.[90] conducted a study involving the creation of a hierarchically porous enzyme@peptide-directed metal–organic framework nanoarchitecture (Fig. 10a). This unique nanostructure was achieved through the introduction of a γ-poly(L-glutamic acid) (PLGA) peptide surface modifier, resulting in both morphological evolution and the formation of defect structures. This modified MOFs-P exhibited expanded pore sizes, providing ample space for enzyme immobilization and facilitating improved substrate diffusion and material communication. These enzyme@peptide-directed MOFs-P played a pivotal role in the development of a plasmonic immunosensor designed for the highly sensitive detection of the imidacloprid pesticide. The enzyme@peptide-directed plasmonic immunosensor exhibited an impressive response and unparalleled selectivity, surpassing traditional immunoassays by a factor of 1000 in terms of sensitivity. Furthermore, the researchers employed a color-based detection method for rapid and precise concentration determination, with the imidacloprid pesticide as the model target. This innovative approach yielded a distinct blue-to-red color shift, enabling precise quantitative analysis through a smartphone-based homemade device and image-processing algorithm. This investigation has significant implications for the advancement of size-controlled nanoarchitectures in cutting-edge biosensors. Fu et al.[94] reported their findings on the synthesis of defective copper-based metal–organic frameworks (Cu-MOFs) achieved by reacting Cu^{2+} ions with 1,3,5-benzene dicarboxylate linkers in the presence of acetic acid (Fig. 10c). These defective Cu-MOFs exhibited enhanced pesticide adsorption kinetics and greater adsorption capacities compared to their pristine counterparts. The researchers developed an efficient dispersive solid-phase extraction method known as Cu-MOFs-6, designed specifically for the rapid extraction of pesticides from food samples. This method allowed for wide-range pesticide detection, boasting low detection limits (ranging from 0.0067 to 0.0164 μg L^{-1}) and impressive recovery rates (ranging from 81.03% to 109.55%) in spiked samples. Their innovative approach addresses the pressing need for efficient pesticide detection in food safety applications. Li and his team[96] conducted comprehensive research on two distinct MOFs, denoted as MOF 1 and MOF 2, each containing an excess of either formic acid or benzoic acid, respectively (Fig. 10b). These MOFs served as versatile platforms with multifaceted functionalities, including sensing, adsorption, and catalytic reduction of chromium Cr(VI) ions. MOF 1, characterized by its fluorescence sensing and impressive Cr(VI) adsorption capabilities, exhibited an ultralow detection limit of 0.0176 ppm and a robust saturated adsorption capacity of 145.77 mg g^{-1}. On the other hand, MOF 2 excelled in the photochemical removal of Cr(VI), achieving a remarkable reduction efficiency of 98.05% within just 70 minutes, maintaining an impressive 92.21% efficiency even after five consecutive photocatalytic cycles. This research showcases the adaptability of defect-rich MOFs for diverse environmental applications, offering a promising solution to environmental pollution challenges.

3.4 Biomedical sensing and health monitoring

The human body is a remarkable ecosystem consisting of complex biological molecules, each playing a crucial role in maintaining health and homeostasis. From DNA and proteins to hormones and metabolites, these biomolecules orchestrate intricate physiological processes essential for our well-being. As the understanding of human biology advances, so does the recognition of the importance of continuous health monitoring. Timely detection of changes in biomolecular profiles can serve as a valuable indicator of potential health issues, allowing for early interventions and personalized healthcare approaches.

Biomedical sensing is crucial for precise biomolecular analysis. The use of defect-rich MOFs to load photosensitive materials for small biomolecule detection has gained recent attention. For instance, Wang et al.[103] introduced a turn-on photoelectrochemical biosensor for highly sensitive protein kinase activity analysis and inhibitor evaluation, relying on

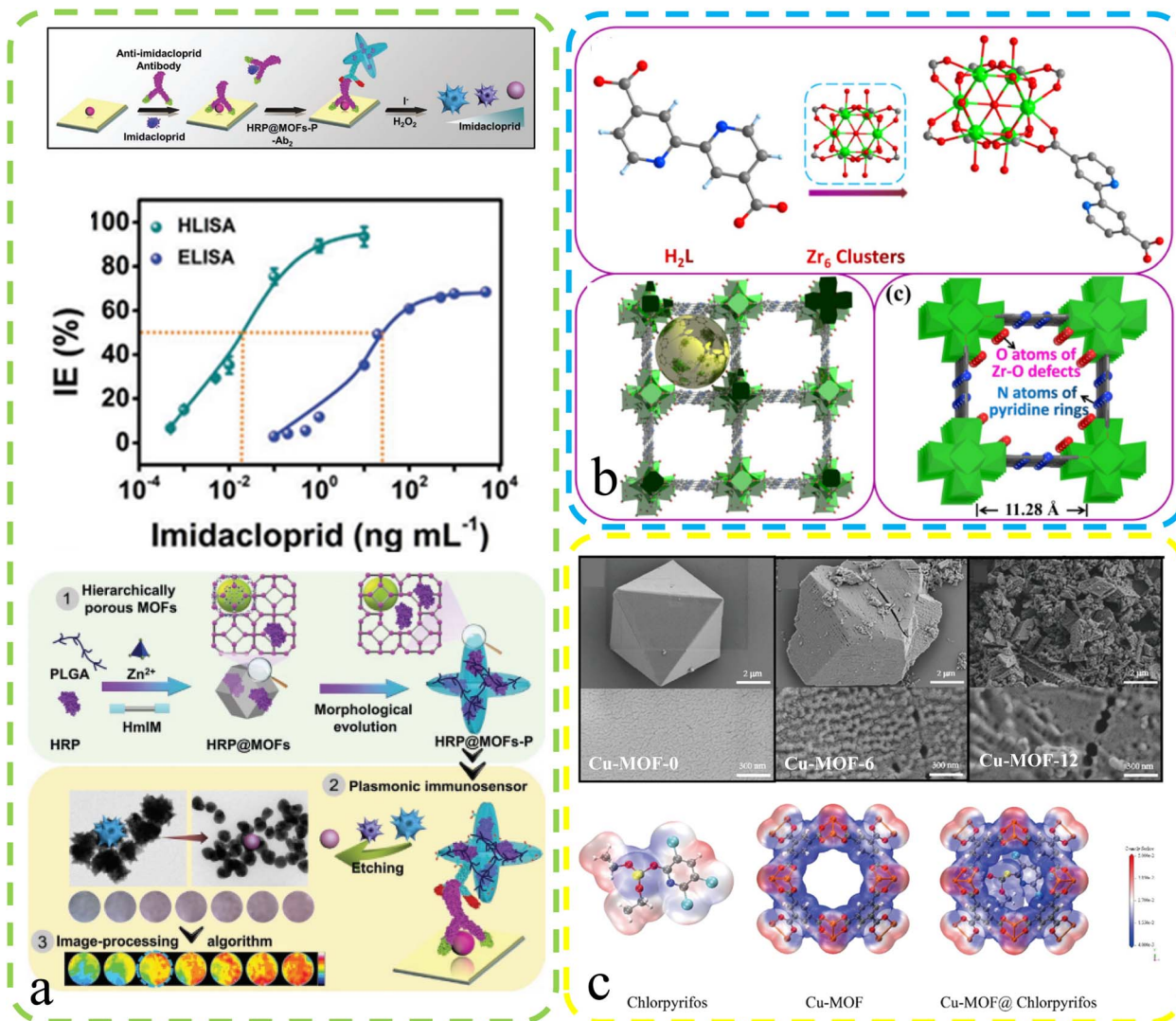**52** | J. Mater. Chem. A, 2024, **12**, 38–58

This journal is © The Royal Society of Chemistry 2024

Fig. 10 (a) Enzyme@MOFs–P plasma immunosensor: defects, mechanism, and performance. Reproduced with permission.[90] Copyright, 2023, Wiley-VCH. (b) Schematic: Zr MOFs 1 assembly *via* repeated units with uncoordinated bipyridyl nitrogen. Reproduced with permission.[96] Copyright, 2021, Royal Society of Chemistry. (c) Top: SEM images for Cu-MOF-0, Cu-MOF-6, and Cu-MOF-12. Bottom: Electron density maps for chlorpyrifos, Cu-MOF and Cu-MOF@chlorpyrifos. Reproduced with permission.[94] Copyright, 2023, Elsevier.

MOFs' surface defect recognition and multiple signal amplification (Fig. 11b). They employed Zr-based UiO-66 MOFs with surface defects, accommodating $[Ru(bpy)_3]^{2+}$ photoactive dyes in their pores. These MOFs were linked to a phosphorylated Kemptide-modified TiO_2/ITO electrode through chelation. Under visible light irradiation, excited electrons from $[Ru(bpy)_3]^{2+}$ in UiO-66 pores are injected into the TiO_2 conduction band, generating photocurrent for kinase activity detection. Defective UiO-66's large surface area and high porosities increased $[Ru(bpy)_3]^{2+}$ and enhanced the photocurrent, enabling sensitive photoelectrochemical analysis with a detection limit of 0.0049 U mL^{-1} (S/N = 3). It was used for kinase inhibitor evaluation and PKA activity detection in MCF-7 cell lysates, promising clinical diagnosis and drug discovery. A carbon dot (CD) material derived through MOF calcination is also widely used for biosensors. Li *et al.*[101] developed CDs@MOFs composites *via* MOF self-carbonization using UiO-

66 type MOFs (UiO-66N) as platforms. They obtained near defect-free and defect-containing UiO-66N through the solvothermal reaction, with defects favoring self-carbonization. CDs@MOFs composites exhibited exceptional luminescence sensing for picric acid, with a high quenching constant (KSV = 4.0×10^5 M^{-1}) and a low limit of detection (LOD: 6.54×10^{-7} M).

Electrodeposition is an important method for enhancing the sensing capabilities of defect-rich MOFs. Chang *et al.*[100] designed electrode materials for electrochemical dopamine (DA) sensing, even in the presence of interferents such as AA and uric acid (UA). They synthesized nanoporous zirconium-based MOFs, UiO-66, with tunable missing-linker defects. A thin film of defective UiO-66 deposited on the electrode surface significantly amplifies the electrochemical sensing signal for DA. This signal enhancement is attributed to the hopping-based electrochemical process of irreversibly adsorbed DA in the

This journal is © The Royal Society of Chemistry 2024

J. Mater. Chem. A, 2024, **12**, 38–58 | **53**

Fig. 11 (a) Top: the electrochemical DA sensor structure – Zr (green), O (red), and C (grey) in UiO-66. Bottom: DPV curves of GO-modified and GO-UiO-66-RT-modified electrodes in 0.5 M KCl with varying DA concentrations. Reproduced with permission.[100] Copyright 2023, American Chemical Society. (b) The configuration of a photoelectrochemical biosensor for kinase activity detection. Reproduced with permission.[103] Copyright, 2020, Nature. (c) Synthesis & microdialysis-electrochemical UA detection with ZIF-L-Co-10 mg cysteine. Reproduced with permission.[98] Copyright 2021, American Chemical Society.

defective MOFs. By using defective UiO-66 as a signal amplifier cast on a graphene oxide (GO) modified electrode, they achieved higher sensitivity (6.4-fold), lower limit of detection (0.23-fold), and better selectivity towards DA against AA and UA (2.6-fold and 1.2-fold, respectively) compared to a GO thin film (Fig. 11a). This approach enhances the sensing performance of electrochemical systems for DA detection. In the study conducted by Guoyuan Ren and colleagues[98] (Fig. 11c), the focus is on enhancing the sensing performance of artificial nanozymes through the manipulation of structural defects in MOFs. The goal is to enhance the catalytic efficiency of nanozymes for accurate biomolecule analysis, addressing limitations such as the high cost and poor stability associated with natural enzymes. Their approach involves using structural defects in

MOFs to regulate the catalytic efficiency of nanozymes. By introducing defects into a Co-containing zeolitic imidazolate framework (ZIF-L-Co) through cysteine doping, catalytic properties are significantly enhanced. Activities such as ascorbate oxidase-like, glutathione oxidase-like, and laccase-like improve over 5, 2, and 3 times, respectively. This improvement can be attributed to sulfur doping disrupting the cobalt–nitrogen equilibrium, enhancing oxygen adsorption and oxidase-like activity. The significance lies in potential sensing applications. Advanced ZIF-L-Co nanozymes are employed in a microreactor integrated into an online electrochemical system. This system eliminates interfering compounds, enabling continuous monitoring of uric acid changes in rat brains after ischemia-

54 | *J. Mater. Chem. A*, 2024, **12**, 38–58

This journal is © The Royal Society of Chemistry 2024

reperfusion injury. This demonstrates the practical utility of defect-tuned nanozymes in biomedical sensing applications.

4. Conclusion and outlook

Defect engineering in MOFs has emerged as a transformative strategy to enhance material properties and tailor their applications across diverse fields. The deliberate introduction of defects offers remarkable opportunities for tuning the structural, electronic, and surface characteristics of MOFs. Controlling defects in MOFs can effectively enhance their adsorption, catalytic conversion, and degradation performance toward pollutants. This paper provides an overview of the distinctions between defective MOFs and regular MOFs and further discusses synthesis methods, specific classifications, and reasons for application, as well as the pros and cons of the DNS and PST for defect engineering in MOFs. Meanwhile, the characterisation of defects in some MOFs is presented. Additionally, the study analyzes synthesis methods and performance modulation strategies for defect-engineered MOFs, along with the current applications of defect-rich MOF sensors in areas such as biosensing, chemical sensing, environmental monitoring, and health diagnostics.

In summary, the development of defect-engineered MOFs has ushered in a new era of understanding regarding the types and concentrations of defects in these materials. This progress is driven by a combination of precise synthesis techniques and cutting-edge characterization tools. Advanced methods such as HRTEM and HRNPD have allowed us to examine defects in unprecedented detail. Emerging techniques, including AFM, CFM, and others, are expanding our ability to study beam-sensitive MOF materials. These advancements in characterization techniques are poised to enhance our comprehension of defects and enable precise quantification.

Controlled synthesis techniques, exemplified by the development of ordered defects in specific MOFs, have brought us closer to the prospect of a universal approach for generating defects. However, it's essential to recognize that when defect engineering offers ways to adjust structural and functional properties, it often involves a trade-off with structural stability. Striking the balance between performance enhancement and stability remains a critical challenge in the design and customization of materials through defect engineering.

The complexity of defects, including their spatial distribution and the proportions of different defect types, presents a central challenge in defect engineering. Herein, computational chemistry emerges as a valuable tool for deciphering the intricate relationship between defects and material properties. Computational methods, such as density functional theory (DFT), are likely to play a more targeted role in the design of defective MOFs for specific applications, guiding experimental synthesis and characterization. The future of defect engineering may see a deliberate integration of computational tools to predict mechanical stability, catalytic mechanisms, and other aspects related to defective MOFs.

To effectively tailor defect-rich MOFs for specific sensing tasks, achieving precision in controlling defect formation and concentration stands as a challenging yet indispensable objective. Fine-tuning these attributes can yield MOFs with unparalleled sensitivity and selectivity, enhancing their effectiveness as sensors. Looking ahead, the synthesis landscape is poised to evolve. Ongoing exploration into advanced synthesis methods, combined with a refined understanding of how structural intricacies correlate with material properties, will undoubtedly lead to groundbreaking progress in defect-based MOFs. The integration of advanced materials such as defective MOFs and sensor technologies holds the promise of reshaping sensing paradigms. By strategically combining the distinctive attributes of defect-rich MOFs with synergistic components, we are on the path to engineering sensors that exhibit exceptional accuracy, responsiveness, and robustness across diverse applications. Furthermore, as researchers continue to forge ahead with determination, pioneering novel synthesis pathways and unraveling the underpinnings of MOFs' functionality, it appears that this field is destined for transformative leaps.

Data availability

The raw data cannot be made public at the request of the affiliated institute.

Author contributions

DA designed the review and prepared the manuscript. YL edited the manuscript and investigated the conceptualization. LC revised the manuscript. All authors contributed to the work and approved the final version of the manuscript.

Conflicts of interest

There are no conflicts to declare.

Acknowledgements

References

1 K. Sun, J. Pang, Y. Zheng, F. Xing, R. Jiang, J. Min, J. Ye, L. Wang, Y. Luo, T. Gu and L. Chen, *J. Alloys Compd.*, 2022, **923**, 166470.

2 C. Fan, X. Zhang, L. Chen, H. Fu, H. Li, J. Hou, F. Yu, H. Li, Y. Shi and X. Guo, *New J. Chem.*, 2019, **43**(38), 15066–15071.

3 J. Pang, H. Fu, W. Kong, R. Jiang, J. Ye, Z. Zhao, J. Hou, K. Sun, Y. Zheng and L. Chen, *Chem. Eng. J.*, 2022, **433**, 133854.

This journal is © The Royal Society of Chemistry 2024

J. Mater. Chem. A, 2024, **12**, 38–58 | **55**

4 H. Li, L. Chen, P. Jin, H. Lv, H. Fu, C. Fan, S. Peng, G. Wang, J. Hou, F. Yu and F. Shi, *Dalton Trans.*, 2020, **49**(20), 6587–6595.

5 H. Li, M. Eddaoudi, M. O'Keeffe and O. M. Yaghi, *Nature*, 1999, **402**(6759), 276–279.

6 C. Ni, H. Zheng, W. Liu, L. Wu, R. Li, K. Zhou and W. Zhang, *Adv. Funct. Mater.*, 2023, 2301075.

7 M. Xiao, C. Wu, J. Zhu, C. Zhang, Y. Li, J. Lyu, W. Zeng, H. Li, L. Chen and S. Mu, *Nano Res.*, 2023, 1–8.

8 D. Wu, W. Yan, H. Xu, E. Zhang and Q. Li, *Inorg. Chim. Acta*, 2017, **460**, 93–98.

9 K. D. Nguyen, N. T. Vo, K. T. M. Le, K. V. Ho, N. T. S. Phan, P. H. Ho and H. V. Le, *New J. Chem.*, 2023, **47**(13), 6433–6447.

10 G. Qu, P. Jia, T. Zhang, Z. Li, C. Chen and Y. Zhao, *Chemosphere*, 2022, **288**, 132594.

11 C. Zhang, C. Han, D. S. Sholland and J. R. Schmidt, *J. Phys. Chem. Lett.*, 2016, **7**(3), 459–464.

12 H. Park, S. Kim, B. Jung, M. H. Park, Y. Kim and M. Kim, *Inorg. Chem.*, 2018, **57**(3), 1040–1047.

13 Z. Wang, J. Huang, W. Wang, X. Wang, Y. Wang, B. Gao and Q. Li, *Chem. Eng. J.*, 2023, **466**, 143194.

14 Y. Song, M. Xu, X. Liu, Z. Li, C. Wang, Q. Jia, Z. Zhang and M. Du, *Electrochim. Acta*, 2021, **368**, 137609.

15 K. Sun, Y. Shen, J. Min, J. Pang, Y. Zheng, T. Gu, G. Wang and L. Chen, *Chem. Eng. J.*, 2023, **454**, 140394.

16 Y. An, S. Dong, Z. He, Q. Xie and T. Huang, *Microchem. J.*, 2022, **172**, 106942.

17 J. Long, Q. Yao, X. Zhang, H. Wu and Z. Lu, *Appl. Catal., B*, 2023, **320**, 121989.

18 B. Yeh, S. Chheda, S. D. Prinslow, A. S. Hoffman, J. Hong, J. E. Perez-Aguilar, S. R. Bare, C. C. C. Lu, L. Gagliardi and A. Bhan, *J. Am. Chem. Soc.*, 2023, **145**(6), 3408–3418.

19 Y. Wu, H. Wang, J. Peng, J. Zhang and M. Ding, *Chem. Eng. J.*, 2023, **454**, 140156.

20 O. Basu, S. Mukhopadhyay, S. Laha and S. K. Das, *Chem. Mater.*, 2022, **34**(15), 6734–6743.

21 Y. Meng, Z. Ma, Y. Huang and Y. Song, *Anal. Sci.*, 2023, 1–9.

22 I. Ahmed, H. J. Lee and S. H. Jhung, *J. Mol. Liq.*, 2021, **344**, 117765.

23 A. K. Kar, R. Sarkar, A. K. Manal, R. Kumar, S. Chakraborty, A. Rajeev and R. Srivastava, *Appl. Catal., B*, 2023, **325**, 122385.

24 L. Pukdeejorhor, S. Wannapaiboon, J. Berger, K. Rodewald, S. Thongratkaew, S. Impeng, J. Warnan, S. Bureekaew and R. A. Fischer, *J. Mater. Chem. A*, 2023, **11**(16), 9143–9151.

25 Z. Fang, B. Bueken, D. E. De Vos and P. D. R. A. Fischer, *Angew. Chem., Int. Ed.*, 2015, **54**(25), 7234–7254.

26 S. Dissegna, K. Epp, W. R. Heinz, G. Kieslich and R. A. Fischer, *Adv. Mater.*, 2018, **30**(37), 1704501.

27 C. H. Shim, S. Oh, S. Lee, G. Lee and M. Oh, *RSC Adv.*, 2023, **13**(12), 8220–8226.

28 Y. Wang and R. Yu, *J. Environ. Chem. Eng.*, 2023, 110422.

29 J. Li, K. K. Lu, L. H. Xu, Y. X. Li, H. Li, G. Shu, X. J. Zhang, R. S. Marks, S. Cosnier and D. Shan, *Analyst*, 2022, **147**(1), 72–79.

30 C. Zhang, X. Zhang, Z. Tao, B. Li, D. Zhao, H. Gao, Z. Zhu, G. Wang and X. Shu, *Chem. Eng. J.*, 2023, **455**, 140487.

31 N. Prasetya and K. Li, *Sep. Purif. Technol.*, 2022, **301**, 122024.

32 Y. Feng, X. Cao, L. Zhang, J. Li, S. Cui, Y. Bai, K. Chen and J. Ge, *Chem. Eng. J.*, 2022, **439**, 135736.

33 Y. Gu, B. A. Anjali, S. Yoon, Y. Choe, Y. G. Chung and D. W. Park, *J. Mater. Chem. A*, 2022, **10**(18), 10051–10061.

34 L. Duan, H. Jiang, W. Wu, D. Lin and K. Yang, *J. Hazard. Mater.*, 2023, **445**, 130426.

35 C. Yang, H. Wu, J. Yun, J. Jin, H. Meng, J. Caro and J. Mi, *Adv. Mater.*, 2023, 2210235.

36 F. Yan, F. Cheng, C. Guo, G. Liang, S. Zhang, S. Fang and Z. Zhang, *J. Colloid Interface Sci.*, 2023, **641**, 59–69.

37 H. Chen, J. Wan, Z. Yan, Y. Ma, Y. Wang, Y. Xie and J. Hou, *J. Cleaner Prod.*, 2022, **348**, 131367.

38 H. An, W. Tian, X. Lu, H. Yuan, L. Yang, H. Zhang, H. Shen and H. Bai, *Chem. Eng. J.*, 2023, **144052.

39 X. Liu, W. Qi, Y. Wang, R. Su and Z. He, *Nanoscale*, 2017, **9**(44), 17561–17570.

40 I. Abánades Lázaro, C. J. R. Wells and R. S. Forgan, *Angew. Chem.*, 2020, **132**(13), 5249–5255.

41 H. Yuan, S. A. Alateeqi Aljneibi, J. Yuan, Y. Wang, H. Liu, J. Fang, C. Tang, X. Yan, H. Cai and Y. Gu, *Adv. Mater.*, 2019, **31**(11), 1807161.

42 M. J. Cliffe, J. A. Hill, C. A. Murray, F. X. Coudert and A. L. Goodwin, *Phys. Chem. Chem. Phys.*, 2015, **17**(17), 11586–11592.

43 G. Zhang, L. Jin, R. Zhang, Y. Bai, R. Zhu and H. Pang, *Coord. Chem. Rev.*, 2021, **439**, 213915.

44 Y. N. Chang, C. H. Shen, C. W. Huang, M. D. Tsai and C. W. Kung, *ACS Appl. Nano Mater.*, 2023, **6**(5), 3675–3684.

45 V. V. Butova, O. A. Burachevskaya, I. V. Ozhogin, G. S. Borodkin, A. G. Starikov, S. Bordiga, A. Damin, K. P. Lillerud and A. V. Soldatov, *Microporous Mesoporous Mater.*, 2020, **305**, 110324.

46 E. Moumen, L. Bazzi and S. El Hankari, *Coord. Chem. Rev.*, 2022, **455**, 214376.

47 M. Peng, D. You, H. Shi, P. Shao, W. Ren, L. Yang, X. Sheng, J. Shao, X. Ding and L. Ding, *Chem. Eng. J.*, 2022, **448**, 137612.

48 P. Wang, L. Sun, J. Ye, Q. Liu, Z. Fei, X. Chen, Z. Zhang, J. Tang, M. Cui and X. Qiao, *Microporous Mesoporous Mater.*, 2021, **312**, 110778.

49 A. A. Tereshchenko, V. V. Butova, A. A. Guda, O. A. Burachevskaya, A. L. Bugaev, A. N. Bulgakov, A. A. Skorynina, Y. V. Rusalev, I. V. Pankov and V. A. Volochaev, *Inorg. Chem.*, 2022, **61**(9), 3875–3885.

50 Y. Shan, G. Zhang, Y. Shi and H. Pang, *Cell Rep. Phys. Sci.*, 2023, **4**(3), 101301.

51 F. Vermoortele, B. Bueken, G. L. Bars, B. V. d. Voorde, M. Vandichel, K. Houthoofd, A. Vimont, M. Daturi, M. Waroquier and V. V. Speybroeck, *J. Am. Chem. Soc.*, 2013, **135**(31), 11465–11468.

52 G. C. Shearer, S. Chavan, S. Bordiga, S. Svelle, U. Olsbye and K. P. Lillerud, *Chem. Mater.*, 2016, **28**(11), 3749–3761.

53 X. Feng, H. S. Jena, K. Leus, G. Wang, J. Ouwehand and P. V. D Voort, *J. Catal.*, 2018, **365**, 36–42.

56 | *J. Mater. Chem. A*, 2024, **12**, 38–58

This journal is © The Royal Society of Chemistry 2024

54 Z. Fan, Z. Wang, M. Cokoja and R. A. Fischer, *Catal. Sci. Technol.*, 2021, **11**(7), 2396–2402.

55 B. N. Truong, D. D. Borges, J. Park, J. S. Lee, D. Jo, J. S. Chang, S. J. Cho, M. Guillaume, K. H. Cho and U. H. Lee, *Adv. Sci.*, 2023, 2301311.

56 J. Zhou, X. Zeng, L. Dong, L. Chen, X. Wei, Y. Liu, L. Shi, L. Yu and J. Fu, *Chem. Eng. J.*, 2023, **466**, 143243.

57 X. C. Zhou, C. Liu, J. Su, Y. F. Liu, Z. Mu, Y. Sun, Z. M. Yang, S. Yuan, M. Ding and J. Zuo, *Angew. Chem., Int. Ed.*, 2023, **62**(10), e202211850.

58 W. Tang, Z. Yu, H. Chen, R. Jiang, J. Huang, S. Li, Y. Hou, M. Wang, H. Pang and J. Liu, *J. Colloid Interface Sci.*, 2023, **644**, 358–367.

59 Y. Cao, X. Mi, X. Li and B. Wang, *Front. Chem.*, 2021, **9**, 673738.

60 K. Epp, I. Luz, W. R. Heinz, A. Rapeyko, X. Li and R. A. Fischer, *ChemCatChem*, 2020, **12**(6), 1720–1725.

61 S. Yu, J. Dong, H. Wang, S. Li, H. Zhu and T. Yang, *J. Mater. Chem. A*, 2022, **10**(48), 25453–25462.

62 J. A. Villajos, N. Jagorel, S. Reinsch and F. Emmerling, *Front. Mater.*, 2019, **6**, 230.

63 A. F. Sapnik, D. N. Johnstone, S. M. Collins, G. Divitini, A. M. Bumstead, C. W. Ashling, P. A. Chater, D. S. Keeble, T. Johnson and D. A. Keen, *Dalton Trans.*, 2021, **50**(14), 5011–5022.

64 S. Chaemchuen, Z. Luo, K. Zhou, B. Mousavi, S. Phatanasri, M. Jaroniec and F. Verpoort, *J. Catal.*, 2017, **354**, 84–91.

65 M. Karimi, H. Mohebali, S. Sadeghi, S. Vahid, A. Mahjoub and A. Heydari, *Microporous Mesoporous Mater.*, 2021, **322**, 111054.

66 R. J. Davey, S. L. M. Schroeder and J. H. Ter Horst, *Angew. Chem., Int. Ed.*, 2013, **52**(8), 2166–2179.

67 G. Ye, H. Wang, X. Zeng, L. Wang and J. Wang, *Appl. Catal., B*, 2021, **299**, 120659.

68 F. N. Shi, Y. Hu, X. Wang, X. Sun, M. Lu, G. Shia and G. Xun, *Dalton Trans.*, 2017, **46**(6), 1936–1942.

69 O. Karagiaridi, N. A. Vermeulen, R. C. Klet, T. C. Wang, P. Z. Moghadam, S. S. Al-Juaid, J. F. Stoddart, J. T. Hupp and O. K. Farha, *Inorg. Chem.*, 2015, **54**(4), 1785–1790.

70 C. T. Lollar, J. S. Qin, J. Pang, S. Yuan, B. Becker and H. C. Zhou, *Langmuir*, 2018, **34**(46), 13795–13807.

71 H. G. T. Nguyen, M. H. Weston, O. K. Farha, J. T. Hupp and S. T. Nguyen, *CrystEngComm*, 2012, **14**(12), 4115–4118.

72 X. Kang, K. Lyu, L. Li, J. Li, L. Kimberley, B. Wang, L. Liu, Y. Cheng, M. D. Frogley and S. Rudić, *Nat. Commun.*, 2019, **10**(1), 4466.

73 G. C. Shearer, J. G. Vitillo, S. Bordiga, S. Svelle, U. Olsbye and K. P. Lillerud, *Chem. Mater.*, 2016, **28**(20), 7190–7193.

74 P. Yang, F. Mao, Y. Li, Q. Zhuang and J. Gu, *Chem. –Eur. J.*, 2018, **24**(12), 2962–2970.

75 J. Szanyi, M. Daturi, G. Clet, D. R. Baerc and C. H. F. Peden, *Phys. Chem. Chem. Phys.*, 2012, **14**(13), 4383–4390.

76 Z. Wang, H. Sezen, J. Liu, C. Yang, S. E. Roggenbuck, K. Peikert, M. Fröba, A. Mavrandonakis, B. Supronowicz and T. Heine, *Microporous Mesoporous Mater.*, 2015, **207**, 53–60.

77 A. F. Zorzo, H. C. Nunes, R. C. Lunardi, R. A. Michelin and S. S. Kanhere, *2018 Eighth Latin-American Symposium on Dependable Computing (LADC)*, IEEE, 2018, pp. 1–9.

78 D. K. Yoo and S. H. Jhung, *Appl. Catal., A*, 2023, **659**, 119170.

79 Y. Zhang, S. Lv, L. Jiang, F. Liu, J. Wang, Z. Yang, B. Wang, R. You, C. Wang and X. Yan, *ACS Sens.*, 2021, **6**(12), 4435–4442.

80 L. Han, P. Qin, M. Li, D. Li, M. Mu, Y. Gao, S. Zhu, M. Lu and Z. Cai, *Chem. Eng. J.*, 2023, **456**, 140969.

81 A. Melillo, M. Cabrero, S. Navalón, M. Álvaro, B. Ferrer and H. García, *Appl. Catal., B*, 2020, **278**, 119345.

82 M. Fu, X. Deng, S.-Q. Wang, F. Yang, L.-C. Lin, M. J. Zaworotko and Y. Dong, *Sep. Purif. Technol.*, 2022, **288**, 120620.

83 H. Sun, G. Song, W. Gong, W. Lu, S. Cong and Z. Zhao, *Nano Res.*, 2022, **15**(6), 5347–5354.

84 Z. Liu, J. Xu, F. Zhang, L. Ji and Z. Shi, *Int. J. Hydrogen Energy*, 2023, **48**(39), 14622–14632.

85 G. Ye, L. Wan, Q. Zhang, H. Liu, J. Zhou, L. Wu, X. Zeng, H. Wang, X. Chen and J. Wang, *Inorg. Chem.*, 2023, **62**(10), 4248–4259.

86 C. Guo, T. Wang, L. Zhang, T. Chen, C. Guo, A. Hassan, N. Akram, Y. Koua and J. Wang, *Nanoscale*, 2022, **14**(41), 15316–15326.

87 S. Gong, Y. Niu, X. Teng, X. Liu, M. Xu, C. Xu, T. J. Meyer and Z. Chen, *Appl. Catal., B*, 2022, **310**, 121333.

88 M. Islamov, P. Boone, H. Babaei, A. J. H. McGaughey and C. E. Wilmer, *Chem. Sci.*, 2023, **14**, 6592–6600.

89 I. G. Koryakina, S. V. Bachinin, E. N. Gerasimova, M. V. Timofeeva, S. A. Shipilovskikh, A. S. Bukatin, A. Sakhatskii, A. S. Timin, V. A. Milichko and M. V. Zyuzin, *Chem. Eng. J.*, 2023, **452**, 139450.

90 X. Yan, D. Su, H. Li, X. Zhao, X. Liu, F. Liu, P. Sun and G. Lu, *Adv. Funct. Mater.*, 2023, 2215192.

91 P. Hu, H. Qin, K. Hu, R. Dai, Z. Wang and K. Huang, *J. Colloid Interface Sci.*, 2022, **628**, 597–606.

92 M. Sha, W. Xu, Y. Wu, L. Jiao, Y. Chen, J. Huang, Y. Tang, W. Gu and C. Zhu, *Sens. Actuators, B*, 2022, **366**, 131927.

93 J.-Y. Tian, X. Liu, S. Zhang, K. Chen, L. Zhu, Y. Song, M. Wang, Z. Zhang and M. Du, *Food Chem.*, 2023, **402**, 134357.

94 Q. Fu, X. Jia, S. Zhang, J. Zhang, D. Sun-Waterhouse, C. Wang, G. I. N. Waterhouse and P. Wu, *Food Chem.*, 2023, **423**, 136319.

95 K. Wu, Y. Yu, Z. Hou, X. Guan, H. Zhao, S. Liu, X. Yang, T. Fei and T. Zhang, *Sens. Actuators, B*, 2022, **355**, 131136.

96 Q. Li, X. Cai, L.-H. Chen, B.-B. Guan, Z.-L. Fan, W. Zhu and D.-X. Xue, *Inorg. Chem.*, 2021, **60**(11), 8143–8153.

97 L.-L. Kang, C. Xing, Y.-X. Jin, L.-X. Xie, Z.-F. Li and G. Li, *Inorg. Chem.*, 2023, **62**(7), 3036–3046.

98 G. Ren, F. Dong, Z. Zhao, K. Li and Y. Lin, *ACS Appl. Mater. Interfaces*, 2021, **13**(44), 52987–52997.

99 R. Zhang, D. Zhang, Y. Yao, Q. Zhang, Y. Xu, Y. Wu, H. Yu and G. Lu, *ACS Appl. Mater. Interfaces*, 2019, **11**(23), 21010–21017.

100 Y.-N. Chang, C.-H. Shen, C.-W. Huang, M.-D. Tsai and C.-W. Kung, *ACS Appl. Nano Mater.*, 2023, **6**(5), 3675–3684.

This journal is © The Royal Society of Chemistry 2024

J. Mater. Chem. A, 2024, **12**, 38–58 | 57

101 L.-X. Li, S. He, S. Zeng, W.-T. Chen, J.-W. Ye, H.-L. Zhou and X.-C. Huang, *J. Mater. Chem. C*, 2023, **11**(1), 321–328.

102 Z. Lu, Y. Jiang, P. Wang, W. Xiong, B. Qi, Y. Zhang, D. Xiang and K. Zhai, *Anal. Bioanal. Chem.*, 2020, **412**, 5273–5281.

103 Z. Wang, Z. Yan, F. Wang, J. Cai, L. Guo, J. Su and Y. Liu, *Biosens. Bioelectron.*, 2017, **97**, 107–114.

104 R. T. Jerozal, T. A. Pitt, S. N. MacMillan and P. J. Milner, *J. Am. Chem. Soc.*, 2023, **145**(24), 13273–13283.

105 S. Karmakar, S. Barman, F. A. Rahimi, D. Rambabu, S. Nath and T. K. Maji, *Nat. Commun.*, 2023, **14**(1), 4508.

106 Z. Jiang, W. Xue, H. Huang, H. Zhu, Y. Sun and C. Zhong, *Chem. Eng. J.*, 2023, **454**, 140093.

107 Y. Liang, Z. Zhang, X. Su, X. Feng, S. Xing, W. Liu, R. Huang and Y. Liu, *Angew. Chem.*, 2023, e202309030.

108 X. Feng, J. Hajek, H. S. Jena, G. Wang, S. K. P. Veerapandian, R. Morent, N. De Geyter, K. Leyssens, A. E. J. Hoffman and V. Meynen, *J. Am. Chem. Soc.*, 2020, **142**(6), 3174–3183.

109 E. Massahud, H. Ahmed, R. Babarao, Y. Ehrnst, H. Alijani, C. Darmanin, B. J. Murdoch, A. R. Rezk and L. Y. Yeo, *Small Methods*, 2023, 2201170.

110 Y. Feng, R. Shi, M. Yang, Y. Zheng, Z. Zhang and Y. Chen, *Angew. Chem.*, 2023, **135**(20), e202302436.

111 M. Shao, Y. Sun, Y. Li, Z. Wu, X. Li, R. Zhang and L. Zhang, *Biosens. Bioelectron.*, 2023, **237**, 115530.

112 C. A. Trickett, K. J. Gagnon, S. Lee, F. Gándara, H.-B. Bürgi and O. M. Yaghi, *Angew. Chem., Int. Ed.*, 2015, **54**(38), 11162–11167.

113 J. Ren, M. Ledwaba, N. M. Musyoka, H. W. Langmi, M. Mathe, S. Liao and W. Pang, *Coord. Chem. Rev.*, 2017, **349**, 169–197.

114 X. Ma, L. Wang, Q. Zhang and H.-L. Jiang, *Angew. Chem., Int. Ed.*, 2019, **58**(35), 12175–12179.

115 G. Cai, X. Ma, M. Kassymova, K. Sun, M. Ding and H.-L. Jiang, *ACS Cent. Sci.*, 2021, **7**(8), 1434–1440.

116 Q. Zheng, X. Liu, S. Gao, Z. Cui, S. Wu, Y. Liang, Z. Li, Y. Zheng, S. Zhu and H. Jiang, *Small*, 2023, 2207687.

117 C. Hu, Y. Bai, M. Hou, Y. Wang, L. Wang, X. Cao, C.-H. Chan, H. Sun, W. Li, J. Ge and K. Ren, *Sci. Adv.*, 2020, **6**(5), eaax5785.

118 M. Bagheri, A. Melillo, B. Ferrer, M. Y. Masoomi and H. Garcia, *ACS Appl. Mater. Interfaces*, 2021, **14**(1), 978–989.

119 Q. Zhao, Q. Du, Y. Yang, Z. Zhao, J. Cheng, F. Bi, X. Shi, J. Xu and X. Zhang, *Chem. Eng. J.*, 2022, **433**, 134510.

120 X. Zhang, D. Zhang, L. Liu, K. Zhang, Y. Zhang, J. Zhao, L. Han, M. Jing, J. Liu and C. Yan, *Chem. Eng. J.*, 2023, **467**, 143360.

121 F. Pambudi, N. Pratiwi and U. Chusnawati, *Mater. Today Commun.*, 2023, **35**, 105967.

122 C. Tong, G. Cai, Y. Yang, T. Wang, Y. Yang, Y. Chen, S. Shi, L. Wu and Y. Guo, *J. Mater. Chem. C*, 2023, **11**(5), 1872–1878.

123 C. Koschnick, R. Stäglich, T. Scholz, M. W. Terban, A. von Mankowski, G. Savasci, F. Binder, A. Schökel, M. Etter and J. Nuss, *Nat. Commun.*, 2021, **12**(1), 3099.

124 X. Zhang, X. Shi, J. Chen, Y. Yang and G. Lu, *J. Environ. Chem. Eng.*, 2019, **7**(5), 103405.

125 X. Zhang, Y. Yang, X. Lv, Y. Wang, N. Liu, D. Chen and L. Cui, *J. Hazard. Mater.*, 2019, **366**, 140–150.

126 J. Chen, M. Zhang, J. Shu, S. Liu, X. Dong, C. Li, L. He, M. Yuan, Y. Wu and J. Xu, *J. Am. Chem. Soc.*, 2023, **145**(43), 23651–23658.

127 Y. Fu, Y. Yao, A. C. Forse, J. Li, K. Mochizuki, J. R. Long, J. A. Reimer, G. De Paëpe and X. Kong, *Nat. Commun.*, 2023, **14**(1), 2386.

128 A. K. Kar, R. Sarkar, A. K. Manal, R. Kumar, S. Chakraborty, R. Ahuja and R. Srivastava, *Appl. Catal., B*, 2023, **325**, 122385.

129 M. Peng, D. You, Z. Jin, C. Ni, H. Shi, J. Shao, X. Shi, L. Zhou, P. Shao, L. Yang and X. Luo, *Environ. Res.*, 2023, **236**, 116752.

130 A. Hartl, S.-H. Park, M. Hoelze, N. Paul and R. Gilles, *J. Solid State Chem.*, 2019, **277**, 290–302.

131 C. Tian, C. Feng and Q. Wang, *Sci. Total Environ.*, 2021, **754**, 142154.

132 M. Gu, M. S. Hyun, M. Han, G. Kim and Y. J. Chang, *Curr. Appl. Phys.*, 2023.

133 S. Guthrie, L. Huelsenbeck, A. Salahi, W. Varhue, N. Smith, X. Yu, L. U. Yoon, J. J. Choi, N. Swami and G. Giri, *Nanoscale Adv.*, 2019, **1**(8), 2946–2952.

134 M. Ostermann and R. Haubner, *Tungsten*, 2023, **5**(1), 136–144.

135 B. Dou, H. Zhang, T. Ye, Q. S. Ma and S. Guo, *Tungsten*, 2023, **5**(1), 189–198.

136 K. Sun, Z. Xiao, Y. Shen, *et al.*, *Nano Res.*, 2023, 1–9.

137 Y. Shen, Y. Liu, K. Sun, *et al.*, *J. Mater. Sci. Technol.*, 2024, **169**, 137–147.

138 J. B. Dong, K. Li, L. X. Gao and C. S. Li, *Tungsten*, 2023, **5**(4), 512–521.

139 Y. Han, Z. H. Liu, C. B. Wu, Y. Zhao, G. Q. Zu, W. W. Zhu and X. Ran, *Tungsten*, 2023, **5**(4), 419–439.

58 | *J. Mater. Chem. A*, 2024, **12**, 38–58

This journal is © The Royal Society of Chemistry 2024